THE JOURNAL OF PHYSICAL CHEMISTRY B
A JOURNAL OF THE AMERICAN CHEMICAL SOCIETY

pubs.acs.org/JPCB

Article

Observation of Long-Lived Charge-Separated States in Anthraquinone−Phenothiazine Electron Donor−Acceptor Dyads: Transient Optical and Electron Paramagnetic Resonance Spectroscopic Studies

Zhibin Yu,◆ Andrey A. Sukhanov,◆ Xiao Xiao,◆ Alessandro Iagatti, Sandra Doria, Valeria Butera, Jianzhang Zhao,* Violeta K. Voronkova,* Mariangela Di Donato,* and Gloria Mazzone*

Cite This: https://doi.org/10.1021/acs.jpcb.3c02723

Read Online

ACCESS | Metrics & More | Article Recommendations | Supporting Information

ABSTRACT: We prepared a series of phenothiazine (PTZ)−anthraquinone (AQ) electron donor−acceptor dyads to study the relationship between molecular structures and the possibility of charge transfer (CT) and intersystem crossing (ISC). As compared to the previously reported **PTZ-AQ** dyad with a direct connection of two units via a C−N single bond, the PTZ and AQ units are connected via a *p*-phenylene or *p*-biphenylene linker. Conformation restriction is imposed by attaching *ortho*-methyl groups on the phenylene linker. UV−vis absorption spectra indicate electronic coupling between the PTZ and AQ units in the dyads without conformation restriction. Different from the previously reported **PTZ-AQ**, thermally activated delayed fluorescence (TADF) is observed for the dyads containing one phenylene linker (**PTZ-Ph-AQ** and **PTZ-PhMe-AQ**). The prompt fluorescence lifetime in cyclohexane is exceptionally long (τ_{PF} = 62.0 ns, population ratio: 99.2%) and 245.0 ns (93.5%) for **PTZ-Ph-AQ** and **PTZ-PhMe-AQ**, respectively (normally τ_{PF} <20 ns); the delayed fluorescence lifetimes for these two dyads were determined as τ_{DF} = 2.4 μs (6.5%) and 7.6 μs (0.8%), respectively. For the dyad containing a biphenylene linker (**PTZ-Ph$_2$Me-AQ**), no TADF was observed. Charge-separated (CS) states were observed for **PTZ-Ph-AQ** and **PTZ-PhMe-AQ**, and the lifetimes were determined as 7.0 and 1.3 μs, respectively, indicating the triplet spin multiplicity of the CS state. The ^{3}CS state lifetimes are shortened to 100 ns and 440 ns for the two dyads, respectively, in the polar solvent acetonitrile. For dyads with a longer linker, i.e., **PTZ-Ph$_2$Me-AQ**, the CS state lifetime is not sensitive to solvent polarity (τ_{CS} = 1.8 and 1.3 μs in cyclohexane and acetonitrile, respectively). In reference dyads, where the PTZ unit is oxidized to sulfoxide, no CT absorption band and TADF were observed, which is attributed to the increased CS state energy (>3 eV) becoming higher than that of the AQ triplet (^{3}AQ*) state (ca. 2.7 eV). These experimental evidence show that the presence of ^{1}CS, ^{3}CS, and ^{3}LE (LE: locally excited) states sharing similar energy is essential for the occurrence of TADF. Population of the long-lived ^{3}CS state (with a lifetime of a few μs) does not produce by itself TADF, because the ISC process of ^{1}CS→^{3}CS is nonsufficient. Femtosecond transient absorption spectra show that charge separation (CS) occurs readily (<5 ps) for most dyads, even in nonpolar solvents. Nanosecond pulsed laser-excited time-resolved electron paramagnetic resonance (TREPR) spectra show that either a spin correlated radical pair (SCRP) is formed, with the electron exchange energy 2J = +2.14 mT, or radical pairs with stronger interaction, |2J| > 6.57 mT. These studies are useful for in-depth understanding of the CS and ISC in compact electron donor−acceptor dyads and for design of efficient TADF emitters.

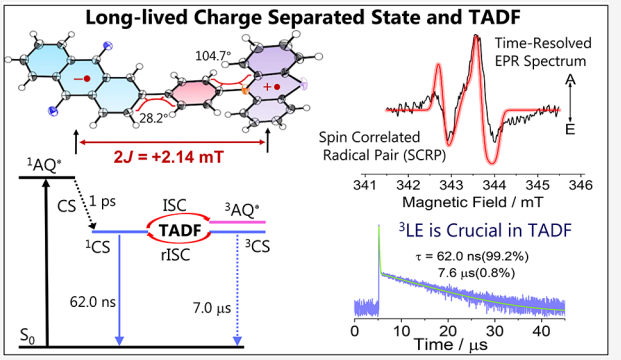

1. INTRODUCTION

Charge separation (CS) and intersystem crossing (ISC) in electron donor−acceptor dyads have been the major topics in photochemistry for decades.[1−12] The study of CS in electron donor−acceptor dyads was usually focused on attaining long-lived CS states to mimic the natural photosynthetic center and for photocatalysis studies.[4,13−18] A long CS state lifetime is usually achieved by reducing the electronic coupling matrix elements between the CS state and the ground state (V_{DA}).[3,19,20] Very often, it is stated as electronic coupling between the donor and acceptor although this is inappropriate. The method is to use a long, rigid, saturated linker between the donor and acceptor although this makes the synthesis difficult.

Received: April 25, 2023
Revised: May 30, 2023

Scheme 1. Molecular Structures and Synthesis of the Compounds[a]

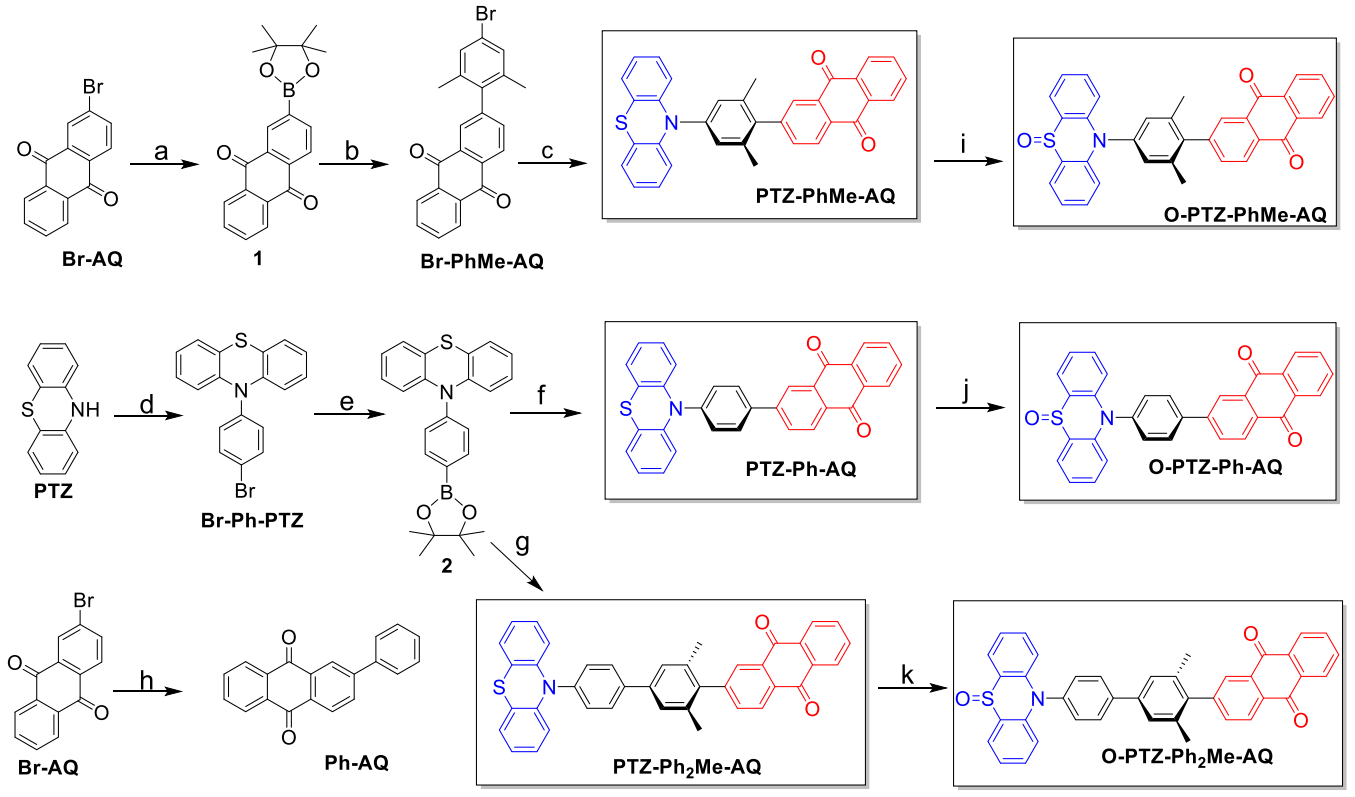

[a]Key: (a) bis(pinacolato)diboron, $PdCl_2(dppf)\cdot CH_2Cl_2$, KOAc, 1,4-dioxane, reflux, 48 h, yield: 64%. (b) 5-bromo-2-iodo-1,3-dimethylbenzene, $Pd(PPh_3)_4$, K_2CO_3, toluene/ethanol/water, 80 °C, 24 h, yield: 51%. (c) phenothiazine, $Pd_2(dba)_3$, tri-*tert*-butyl phosphine, sodium *tert*-butoxide, toluene, 120 °C, 12 h, yield: 41%. (d) 1-bromo-4-iodobenzene, $CuSO_4\cdot 5H_2O$, K_2CO_3, 1,2-dichlorobenzene, 180 °C, 24 h, yield: 43%. (e) bis(pinacolato)diboron, $PdCl_2(dppf)\cdot CH_2Cl_2$, KOAc, 1,4-dioxane, reflux, 11 h, yield: 40%. (f) 2-bromoanthraquinone, $Pd(PPh_3)_4$, K_2CO_3, toluene/ethanol/water, 80 °C, 24 h, yield: 53%. (g) **Br-PhMe-AQ**, $Pd(PPh_3)_4$, K_2CO_3, toluene/ethanol/water, 80 °C, 24 h, yield: 38%. (h) phenylboronic acid, $Pd(PPh_3)_4$, 2 M K_2CO_3, toluene, 130 °C, 12 h, yield: 50%. (i) H_2O_2, acetic acid, RT, 1.5 h, yield: 37%. (j) H_2O_2, acetic acid, RT, 1.5 h, yield: 39%. (k) H_2O_2, acetic acid, RT, 1.5 h, yield: 32%.

The observation of long-lived CS states in compact donor−acceptor dyads is still challenging because of the large V_{DA} values and the expected fast charge recombination (CR) to the ground state.[3] Pushing the CR to the Marcus inverted region is also useful for attaining long-lived CS states and it has a profound effect on the photophysical pathways.[21−23] Recently, a novel approach was proposed to prolong the CS state lifetime, i.e., the electron spin control method.[3,6,24−31] Because both the CS and CR are electron spin selective, the ^{1}LE → ^{1}CS (LE: locally excited) prevails over the ^{1}LE → ^{3}CS. ^{1}CS → S_0 is generally faster than ^{3}CS → S_0; thus, given the ^{3}CS state is formed, its lifetime is longer than the corresponding ^{1}CS state. A few methods have been proposed to populate the ^{3}CS state, for instance, by intermolecular triplet photosensitizing,[32] or by using chromophores showing ultrafast ISC, such as transition metal complexes (^{1}MLCT → ^{3}MLCT ultrafast ISC occurs),[27,29] or using the recently developed spin−orbit charge transfer ISC (SOCT-ISC) in a compact orthogonal dyad.[33,34] In the latter case, the π-conjugation planes of the donor and acceptor adopt orthogonal or perpendicular geometry, so that the total angular momentum is conserved by off-setting the electron spin angular momentum change of the ISC with the molecular orbital angular momentum change during CS or CR.[35−40] Thus, a long-lived ^{3}CS state can form with a triplet LE state (^{3}LE) as the precursor of CS. For these molecular systems, the critical issue is to manipulate the ^{1}CS, ^{3}CS, and ^{3}LE states, concerning both the energy levels and the competing photophysical pathways. Moreover, it is still controversial whether the ^{1}CS and ^{3}CS states can be discriminated by transient absorption spectroscopy since their spectral features appear often very similar. Under ideal circumstances, the molecular orbital occupancy is literally the same for both ^{1}CS and ^{3}CS states, with the radical anion localized on the acceptor and radical cation confined on the donor. The electronic absorption of the ^{1}CS state, i.e., the sum of the absorption bands of the $D_0^+ \rightarrow D_n^+$ transition confined on the donor (radical cation) and the $A_0^- \rightarrow A_n^-$ transition confined on the acceptor (radical anion) are the same as compared to the electronic absorption of the ^{3}CS state, making it difficult to discriminate between these two states by transient optical absorption spectroscopic methods.[37,41] Although our recent study shows that this is not always the case, clearly more examples are needed to elucidate this issue.

Manipulation of the ^{1}CS, ^{3}CS, and ^{3}LE states in electron donor−acceptor dyads is also meaningful to design organic optical materials, such as electron donor−acceptor dyads for thermally activated delayed fluorescence (TADF).[42−47] These systems can be used as OLED materials because both the singlet and triplet excitons can be harvested by TADF materials for light emitting, and the internal quantum efficiency can be up to 100%. However, in-depth investigation of the detailed photophysical processes involved in TADF is

https://doi.org/10.1021/acs.jpcb.3c02723
J. Phys. Chem. B XXXX, XXX, XXX−XXX

rare.[48−50] Initially, a two-state model was used to explain TADF, but recently, a three-state model has been proposed,[51,52] considering three states, ^{1}CS, ^{3}CS, and ^{3}LE as involved in the TADF process. It was further proposed that the ^{3}LE state is an essential intermediate state, by which the spin−vibronic coupling enhances the reverse ISC (rISC) for TADF.[53−57] However, direct experimental evidence for these theories is rare.[41]

In order to study the above-mentioned photophysical processes in compact electron donor−acceptor dyads, herein, we prepared a series of phenothiazine (PTZ)−anthraquinone (AQ) dyads (Scheme 1), with *p*-phenylene or *p*-biphenylene linkers between the two units, to tune the electronic coupling magnitude as well as the energy of the CS state. Methyl groups were furthermore attached on the phenylene linker to impose conformation restriction. TADF was observed for the dyads with a prompt fluorescence lifetime of up to 245 ns. Our compounds represent a rare class of TADF emitters: there are two ^{3}LE states, i.e., ^{3}AQ* and ^{3}PTZ* states, whose energies are 2.7 and 2.6 eV, respectively, close to the CS state energy. Long-lived ^{3}CS states were observed with nanosecond transient absorption spectroscopy. Direct experimental evidence shows that the population of the long-lived ^{3}CS state is nonsufficient to produce TADF. DFT computations suggest that the geometry of the PTZ unit can aid in the assignment of the transient species as the ^{3}LE state or the ^{3}CS state. Femtosecond transient absorption and nanosecond time-resolved electron paramagnetic resonance (TREPR) spectroscopic methods were also used to characterize the dyads.

2. EXPERIMENTAL SECTION

2.1. General Method. All chemicals used for synthesis were analytically pure. Solvents for synthesis were freshly dried before use. ^{1}H and ^{13}C NMR spectra were recorded on Bruker 400 MHz (600 MHz) and 125 MHz spectrometers, respectively. HRMS (high-resolution mass spectrometry) was recorded by an EI-TOF-HRMS spectrometer. The UV−vis absorption spectra were obtained with a UV-2550 spectrofluorometer (Shimadzu Ltd., Japan). The fluorescence emission spectra were recorded on an FS5 spectrophotometer (Edinburgh Instruments Ltd., U.K.). The absolute fluorescence quantum yields (Φ_F) were measured with an absolute photoluminescence quantum yield spectrometer (Quantaurus-QY Plus C13534-11, Hamamatsu Photonics Ltd., Japan). The fluorescence lifetimes were recorded on an OB920 luminescence lifetime spectrometer (Edinburgh Instrument Ltd., U.K.), and the excitation sources are the 340 nm (max. pulse width is 95 ps) EPL picosecond pulsed diode laser. A deconvolution analysis was used for fitting the short fluorescence lifetimes with the instrumental response function (IRF) included. The typical IRF of the luminescence lifetime measurement was 100 ps.

2.2. Compound PTZ-Ph-AQ.[58] Compound **2** (100 mg, 0.25 mmol), 2-bromoanthraquinone (100 mg, 0.35 mmol), and potassium carbonate (104 mg, 0.75 mmol) were dissolved in a mixed solvent of toluene (2.5 mL)/ethanol (0.8 mL)/water (0.4 mL). The mixture was purged with N_2 for 15 min, and then, the catalyst $Pd(PPh_3)_4$ (29 mg, 0.02 mmol) was added. The reaction mixture was stirred at 78 °C under N_2 for 24 h. After completion of the reaction, the reaction mixture was cooled to room temperature. The reaction mixture was poured into water (30 mL), and the mixture was extracted with chloroform (3 × 30 mL). The combined organic layer was dried by anhydrous Na_2SO_4. Then, the solvent was removed under reduced pressure, and the residue was purified by column chromatography (silica gel, petroleum ether/dichloromethane = 2/1, v/v) to obtain an orange solid (64 mg, yield: 53%). Mp: 204.2−205.7 °C. ^{1}H NMR ($CDCl_3$, 400 MHz): δ 8.61 (d, 1 H, J = 1.9 Hz), 8.42 (d, 1 H, J = 8.1 Hz), 8.37−8.34 (m, 2 H), 8.10−8.07 (m, 1 H), 7.92 (d, 2 H, J = 8.4 Hz), 7.84−7.82 (m, 2 H), 7.50 (d, 2 H, J = 8.4 Hz), 7.12−7.10 (m, 2 H), 6.97−6.87 (m, 4 H), 6.45 (d, 2 H, J = 8 Hz). ^{13}C NMR ($CDCl_3$, 125 MHz): δ 183.14, 182.80, 145.81, 137.78, 134.26, 134.12, 134.04, 133.68, 133.62, 132.35, 132.22, 129.51, 128.21, 127.33, 127.28, 126.96, 125.53, 117.67. HRMS ($C_{32}H_{19}NO_2S$ + H^+): calcd m/z = 482.1215; found m/z = 482.1191.

2.3. Compound PTZ-Ph$_2$Me-AQ.[58] **PTZ-Ph$_2$Me-AQ** was prepared by a similar method used for **PTZ-Ph-AQ**. The purple solid was obtained (55 mg, yield: 38%). Mp: >250 °C. ^{1}H NMR ($CDCl_3$, 600 MHz,): δ 8.43 (d, 1 H, J = 7.8 Hz), 8.38−8.34 (m, 2H), 8.20 (s, 1 H), 7.88−7.83 (m, 4 H), 7.68 (d, 1 H, J = 7.8 Hz), 7.46 (s, 4 H), 7.06 (d, 2 H, J = 6.5 Hz), 6.84 (s, 4 H), 6.28 (s, 2 H), 2.15 (s, 6 H). ^{13}C NMR ($CDCl_3$, 125 MHz): δ 183.26, 183.01, 147.45, 140.58, 139.82, 139.37, 136.20, 135.19, 134.22, 134.15, 133.81, 133.67, 132.32, 129.36, 128.05, 127.76, 127.29, 126.88, 126.53, 116.39, 21.02. HRMS ($C_{40}H_{27}NO_2S$): calcd m/z = 585.1762; found m/z = 585.1736.

2.4. Compound PTZ-PhMe-AQ.[59] **Br-PhMe-AQ** (100 mg, 0.26 mmol), phenothiazine (60 mg, 0.31 mmol), $Pd_2(dba)_3$ (6.85 mg, 0.75 mmol %), and sodium *tert*-butoxide (120 mg, 1.25 mmol) were mixed in dry toluene (5 mL). The mixture was purged with N_2 for 15 min, and then, tri-*tert*-butyl phosphine (0.04 mL, 0.02 mmol) was added by a syringe under a N_2 atmosphere. The reaction mixture was stirred at 120 °C under N_2 for 12 h. After completion of the reaction, the reaction mixture was cooled to room temperature. The reaction mixture was poured into water (30 mL), and the mixture was extracted with dichloromethane (3 × 30 mL). The combined organic layer was dried over anhydrous Na_2SO_4. Then, the solvent was removed under reduced pressure, and the residual was purified by column chromatography (silica gel, petroleum ether/dichloromethane = 3/1, v/v) to obtain a red solid (55 mg, yield 41%). Mp: 240.4−241.4 °C. ^{1}H NMR ($CDCl_3$, 400 MHz): δ 8.45 (d, 1 H, J = 7.9 Hz), 8.39−8.35 (m, 2 H), 8.22 (d, 1 H, J = 1.6 Hz), 7.85−7.83 (m, 2 H), 7.73−7.71 (m, 1 H), 7.18 (s, 2 H), 7.05−7.02 (m, 2 H), 6.95−6.91 (m, 2 H), 6.84−6.82 (m, 2 H), 6.38 (d, 2 H, J = 8.1 Hz), 2.11 (s, 6 H). ^{13}C NMR ($CDCl_3$, 125 MHz): δ 183.22, 182.95, 147.02, 144.16, 140.52, 139.68, 138.33, 135.10, 134.28, 134.19, 133.87, 133.65, 133.62, 132.43, 129.36, 128.03, 127.85, 127.33, 127.31, 126.89, 126.78, 122.56, 120.50, 116.34, 20.97. HRMS ($C_{34}H_{23}NO_2S$ + H^+): calcd m/z = 510.1528; found m/z = 510.1502.

2.5. Compound O-PTZ-Ph-AQ.[60] **PTZ-Ph-AQ** (63 mg, 0.13 mmol) was dissolved in acetic acid (6.7 mL). H_2O_2 (0.26 mL, 30%, 2.6 mmol) was added dropwise. The mixture was stirred for 1.5 h at room temperature. After the reaction was completed, the reaction mixture was poured into water (30 mL), and then the mixture was extracted with dichloromethane (3 × 30 mL). The combined organic layer was dried over anhydrous Na_2SO_4. Then, the solvent was removed under reduced pressure, and the residue was purified by column chromatography (silica gel, ethyl acetate/dichloromethane = 1/1, v/v) to obtain a yellow solid (25 mg, yield: 39%). Mp: >250 °C. ^{1}H NMR (DMSO-d_6, 400 MHz): δ 8.60 (d, 1 H, J = 1.6 Hz), 8.45−8.43 (m, 1 H), 8.38 (d, 1 H, J = 8.0 Hz), 8.31−

https://doi.org/10.1021/acs.jpcb.3c02723
J. Phys. Chem. B XXXX, XXX, XXX−XXX

8.27 (m, 4 H), 8.10−8.07 (m, 2 H), 8.00−7.98 (m, 2 H), 7.68 (d, 2 H, J = 8.4 Hz), 7.60−7.56 (m, 2 H), 7.35−7.32 (m, 2 H), 6.80 (d, 2 H, J = 8.5 Hz). ^{13}C NMR ($CDCl_3$, 125 MHz): δ 183.03, 182.74, 145.33, 140.31, 139.93, 138.80, 134.37, 134.24, 134.14, 133.66, 133.60, 132.79, 132.66, 132.46, 131.97, 131.39, 130.19, 128.34, 127.40, 127.34, 125.85, 122.77, 122.31, 117.27. HRMS ($C_{32}H_{19}NO_3S$ + H^+): calcd m/z = 498.1086; found m/z = 498.1156.

2.6. Compound O-PTZ-PhMe-AQ.[60] **O-PTZ-PhMe-AQ** was prepared by a similar method used for **O-PTZ-Ph-AQ**. The yellow solid was obtained (25 mg, yield: 37%). Mp: >250 °C. ^{1}H NMR ($CDCl_3$, 400 MHz): δ 8.50 (d, 1 H, J = 7.9 Hz), 8.40−8.37 (m, 2 H), 8.26 (s, 1 H), 8.03 (d, 2 H, J = 7.5 Hz), 7.87−7.85 (m, 2 H), 7.77 (d, 1 H, J = 7.1 Hz), 7.54−7.50 (m, 2 H), 7.31−7.29 (m, 2 H), 7.25 (s, 2 H), 6.92 (d, 2 H, J = 8.5 Hz), 2.15 (s, 6 H). ^{13}C NMR ($CDCl_3$, 125 MHz): δ 183.17, 182.88, 146.50, 141.18, 139.10, 138.88, 138.72, 134.90, 134.37, 134.27, 134.02, 133.65, 133.62, 132.67, 131.88, 129.24, 128.02, 127.90, 127.38, 122.23, 122.12, 117.54, 20.98. HRMS ($C_{34}H_{23}NO_3S$ + H^+): calcd m/z = 526.1399; found m/z = 526.1466.

2.7. Compound O-PTZ-Ph$_2$Me-AQ.[60] **O-PTZ-Ph$_2$Me-AQ** was prepared by a similar method used for **O-PTZ-Ph-AQ**. The yellow solid was obtained (25 mg, yield: 32%). Mp: >250 °C. ^{1}H NMR ($CDCl_3$, 400 MHz): δ 8.45 (d, 1 H, J = 7.9 Hz), 8.39−8.35 (m, 2 H), 8.21 (s, 1 H), 8.03 (d, 2 H, J = 7.5 Hz), 7.96 (d, 2H, J = 8.0 Hz), 7.85−7.83 (m, 2 H), 7.69 (d, 1 H, J = 8.0 Hz), 7.53−7.43 (m, 6 H), 7.28 (s, 1 H), 7.25 (s, 1 H), 6.84 (d, 2 H, J = 8.5 Hz), 2.17 (s, 6 H,). ^{13}C NMR ($CDCl_3$, 125 MHz): δ 183.26, 182.98, 147.34, 142.18, 139.81, 139.44, 139.01, 138.54, 136.41, 135.15, 134.25, 134.18, 133.90, 133.73, 132.61, 132.43, 131.93, 130.87, 129.85, 129.30, 128.03, 127.82, 127.32, 126.65, 122.16, 117.53, 117.44, 21.03. HRMS ($C_{40}H_{27}NO_3S$ + H^+): calcd m/z = 602.1712; found m/z = 602.1776.

2.8. Electrochemical Studies. The cyclic voltammograms were recorded with a CHI610D electrochemical workstation (CHI instruments, Inc., Shanghai, China). In N_2-purged saturated dichloromethane solutions containing 0.10 M $Bu_4N[PF_6]$ as a supporting electrolyte, platinum electrode was used as the counter electrode, the glassy carbon electrode was used as the working electrode, and $Ag/AgNO_3$ (0.1 M in ACN) couple was used as the reference electrode. Ferrocenium/ferrocene (FcH/FcH^+) redox couple was used as an internal reference. Spectroelectrochemistry was performed using a 0.1 cm path length quartz electrochemical cell. The gauze platinum as the working electrode, platinum wire as the counter electrode, and $Ag/AgNO_3$ as the reference electrode were equipped in the cell. $Bu_4N[PF_6]$ was used as the supporting electrolyte. The potential was regulated with the CHI610D electrochemical workstation (CHI instruments, Inc., Shanghai, China), and the spectra were recorded with an Agilent 8453E UV/Vis spectrophotometer (Agilent Technologies Inc.). Samples were deaerated with N_2 for ca. 5 min before the measurement, and the N_2 atmosphere was kept during the measurement.

2.9. Nanosecond Transient Absorption Spectroscopy. The nanosecond transient absorption spectra were measured on an LP980 laser flash photolysis spectrometer (Edinburgh Instruments, Ltd., U.K.). The data (kinetic decay traces and the transient difference absorption spectra) were analyzed by L900 software. All samples were deaerated with N_2 for ca. 15 min before the measurement. Collinear configuration of the pump and probe beams was used. The sample solution was excited with a nanosecond pulsed laser (Opolette 355II+UV nanosecond pulsed laser. OPOTEK). The typical laser pulse energy was 5 mJ per pulse.

2.10. Femtosecond Transient Absorption Spectra. Pump−probe experiments were performed on a setup based on a regenerative amplifier Ti:sapphire laser (Legend, Coherent), pumped by a Ti:sapphire oscillator (Micra, Coherent). The system produced 40 fs pulses at 800 nm at 1 kHz repetition rate with an average 3.2 W power. The pump pulses at 350 nm were obtained by the second harmonic generation of the 700 nm signal beam produced by sending a portion of the fundamental laser radiation to a commercial optical parametric amplifier (Topas, Light Conversion). The probe beam has been obtained by focusing another small portion of the fundamental laser output on a 3 mm thick calcium fluoride window, generating a white light continuum covering the 375−750 nm spectral window. The white light was then split in a probe and reference beam using a 50% beam splitter. Pump−probe delays were introduced by sending the fraction of the pulse used to generate the white light to a motorized translation stage. Both the pump and probe were spectrally overlapped at the sample position, and after crossing into the sample, the probe and reference beams were sent through a spectrograph coupled to a homemade detector. The sample solution was contained in a 2 mm quartz cuvette, mounted on a movable stage to avoid photodegradation and multiple excitations. The data were analyzed by means of singular value decomposition and global analysis by employing the software Glotaran.[61]

2.11. Time-Resolved Electron Paramagnetic Resonance (TREPR) Spectroscopy. TREPR measurements were performed with an X-band EPR Elexsys E-580 spectrometer. The sample was dissolved in toluene at room temperature. O_2 was removed by a few freeze−pump−thaw cycles. The sample was excited by a pulsed laser with 1 mJ energy per pulse at 355 nm. The EasySpin program package based on MATLAB was used to analyze the data.[62]

2.12. Single-Crystal X-ray Diffraction Analysis. The single crystals of the compounds were obtained via slow evaporation of an n-hexane (HEX)/dichloromethane (DCM) solution. Reflection data were collected at 120 K on a Bruker AXS SMART APEX II CCD diffractometer with graphite-monochromatized Mo Kα radiation (λ = 0.71073 Å). The data were acquired using the SMART and SAINT programs. The structure was solved by direct methods and refined by full-matrix least-squares methods by the program Olex2.[63] In the structural refinement, all of the nonhydrogen atoms were refined anisotropically. The hydrogen atoms within the structure were fixed geometrically at calculated distances and allowed to ride on the parent nonhydrogen atoms. CCDC No. 2160474 (**PTZ-Ph-AQ**), CCDC No. 2155102 (**PTZ-PhMe-AQ**), and CCDC No. 2155103 (**PTZ-Ph$_2$Me-AQ**) contain the supplementary crystallographic data for this paper, and the data can be obtained freely from the Cambridge Crystallographic Data Centre.

2.13. Computational Details. DFT and its TD extension were used to explore the structural and photophysical properties of the synthesized molecules. The ground-state S_0 molecular structure of the dyads was in the optimized gas phase at B3LYP/6-31G* level of theory. TD-DFT in implicit solvent was thus used to compute the excitation energy and triplet state energy as well as to optimize the excited state

https://doi.org/10.1021/acs.jpcb.3c02723
J. Phys. Chem. B XXXX, XXX, XXX−XXX

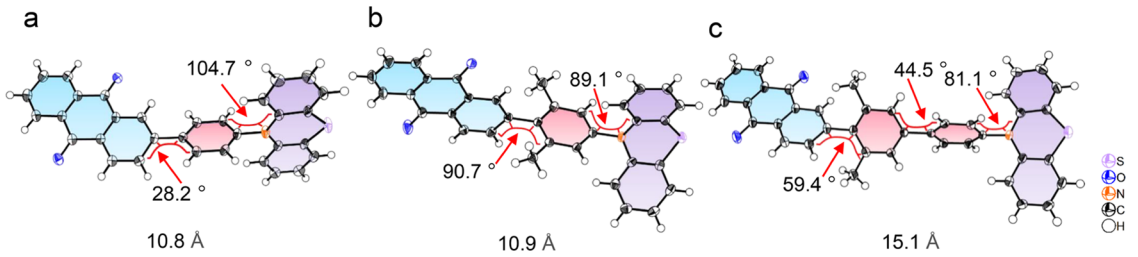

Figure 1. ORTEP of the molecular structure of (a) **PTZ-Ph-AQ**, (b) **PTZ-PhMe-AQ**, and (c) **PTZ-Ph$_2$Me-AQ** determined by single-crystal X-ray diffraction. Thermal ellipsoids are at 50% probability. CCDC numbers: (a) 2160474, (b) 2155102, and (c) 2155103 contain detailed information. The centroid-to-centroid distances (in Å) between the PTZ and the AQ units are also presented at the bottom.

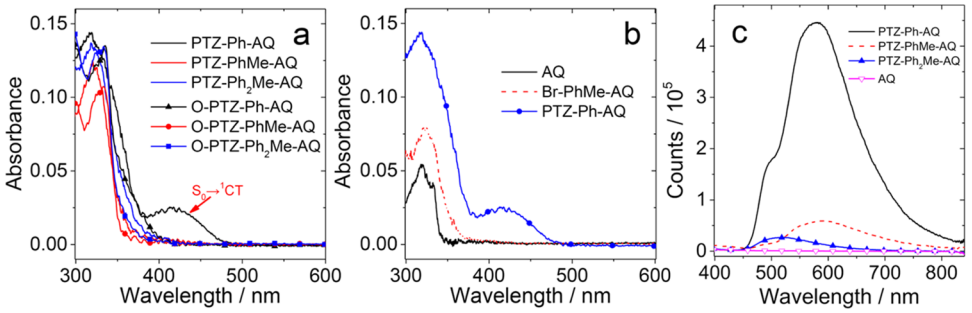

Figure 2. (a, b) UV−vis absorption spectra of the compounds. $c = 1.0 \times 10^{-5}$ M in HEX. (c) Comparison of the fluorescence emission spectra of the compounds; optically matched solutions were used for comparison of the emission, $\lambda_{ex} = 320$ nm, $A = 0.105$, in cyclohexane (CHX), 20 °C.

structures. TD-DFT is a well-established method to investigate the photophysical properties of different materials;[64−66] nevertheless, in some cases, substantial errors can result when calculating excitation energies using the standard exchange−correlation functionals. Given the importance of the energy gaps in radiationless ISC and rISC processes, to avoid this inconsistency, we have used an optimally tuned range-separated functional, referred to as LC-BLYP*, with a determined range separation parameter γ derived from the ionization potential of N and N+1 electron systems, accordingly to what was previously reported,[67] and benchmarked our protocol against the available experimental data. Moreover, the Tamm−Dancoff approximation (TDA)[68] has been introduced as it significantly improves the accuracy of triplet state energy and then ΔE_{ST} values.[69−71] Therefore, TDA-TD-DFT calculations have been performed to calculate the singlet/triplet excitation energies along with the singlet−triplet energy gaps relevant to the TADF process. The polarizable continuum model (PCM) has been used to perform self-consistent reaction field calculations, considering one of the solvents used in the experiments, cyclohexane (ε = 2.0165).

The ISC for singlet state deactivation was evaluated by computing the spin−orbit matrix elements as previously reported[72] for the selected deactivation channels. Most of the computations were performed using the Gaussian 16 package, with the exception of spin−orbit coupling (SOC) that was computed with ORCA software.

3. RESULTS AND DISCUSSION

3.1. Molecular Structure Design and Synthesis. In order to obtain a long-lived ^{3}CS state in compact donor−acceptor dyads, we built a bichromophoric system, where AQ is used as an electron acceptor (Scheme 1) due to its ultrafast ISC (0.4 ps) and high triplet energy (2.7 eV)[73] and the phenothiazine (PTZ) unit is used as an electron donor. Previously, a **PTZ-AQ** dyad with a direct connection of two units via a C−N bond was reported.[74,75] Herein, we synthesized PTZ-AQ compact donor−acceptor dyads with *p*-phenylene or *p*-biphenylene linkers between the PTZ and the AQ units (Scheme 1) to tune the electronic coupling magnitude as well as the energy of the CS state by increasing the distance between the donor and acceptor. We also tuned the redox potentials of the PTZ unit by oxidizing it to a sulfoxide structure, a weaker electron donor than the pristine PTZ unit, to invert the energy level ordering of the LE and CS states.[75] Furthermore, increasing the distance between the donor and acceptor may increase the reorganization energy and affect the electron transfer dynamics.[76] The synthesis of the dyads was carried out with the Suzuki−Miyaura cross-coupling reactions and Buchwald−Hartwig coupling reaction (Scheme 1). The yields of the compounds were satisfactory, and the molecular structures were fully characterized by ^{1}H NMR, ^{13}C NMR, and HRMS spectroscopic methods.

Single crystals of the compounds were obtained via slow evaporation of an *n*-hexane (HEX)/dichloromethane (DCM) solution. The structures obtained for the PTZ-AQ series of compounds are shown in Figure 1. The torsion angles between the electron donor PTZ and the phenylene linker are 104.7, 89.1, and 81.1° in the three dyads, respectively. The torsion angles are similar to those calculated by DFT and different from the previously reported **PTZ-AQ** dyad with a direct connection between PTZ and AQ via a C−N bond (81.6°). Moreover, we found that the PTZ moiety in the dyad adopts a slightly puckered geometry.[77] The distortion angles of the PTZ moieties in the three dyads are 3.0, 33.9, and 24.1°, respectively. The dihedral angles between the AQ and PTZ moieties in the three dyads are 77.3, 20.2, and 31.4°, respectively. The centroid-to-centroid distance between the donor and acceptor are 10.8, 10.9, and 15.1 Å, respectively.

3.2. UV−Vis Absorption and Fluorescence Emission Spectra. The UV−vis absorption spectra of the compounds

https://doi.org/10.1021/acs.jpcb.3c02723
J. Phys. Chem. B XXXX, XXX, XXX−XXX

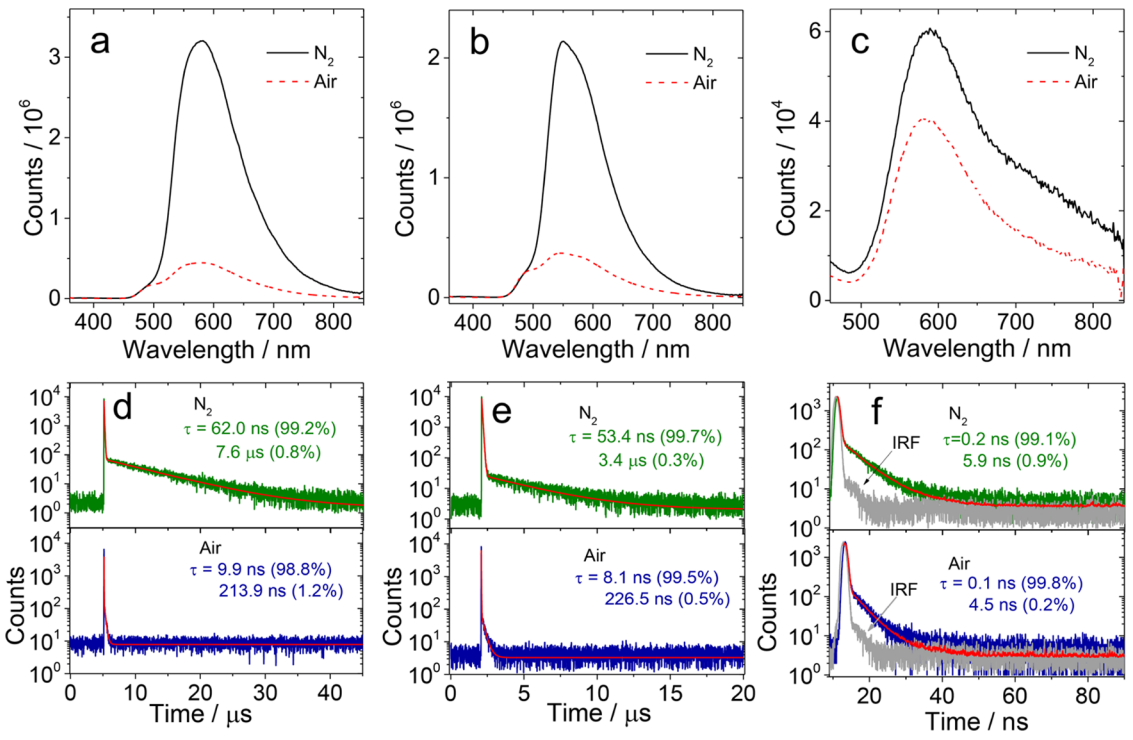

Figure 3. Fluorescence emission spectra of **PTZ-Ph-AQ** in (a) CHX, (b) HEX, and (c) toluene (TOL) under different atmospheres (N_2, air). Optically matched solutions were used, λ_{ex} = 320 nm, A = 0.105. Fluorescence decay traces of **PTZ-Ph-AQ** at 580 nm in (d) CHX ($E_T(30)$ = 30.9 kcal mol^{-1}), (e) HEX ($E_T(30)$ = 31.0 kcal mol^{-1}), and (f) TOL ($E_T(30)$ = 33.9 kcal mol^{-1}), under different atmospheres (N_2, air), respectively. c = 1.0 × 10^{-5} M, λ_{ex} = 340 nm. 20 °C. IRF represents instrument response function.

are presented in Figure 2a. The reference compound **AQ** has an absorption band at 320 nm, similar to that of the reference compound **Br-PhMe-AQ**, except for the tail on the lower energy side of the band (Figure 2b). Interestingly, **PTZ-Ph-AQ** shows a weak, broad, structureless absorption band centered at 418 nm, which is not observed for **Ph-AQ** (Figure S25). We propose that the PTZ and AQ units are electronically coupled in **PTZ-Ph-AQ**,[78−81] even if the two units are separated by an intervening phenylene linker. This conclusion is supported by the lack of a similar absorption band at 418 nm in the UV−vis absorption spectrum of **PTZ-PhMe-AQ**, in which the dihedral angle between the AQ and the intervening phenylene moiety (90.7°) is larger than that in **PTZ-Ph-AQ** (28.2°). This result demonstrates that the conformation restriction imposed by the methyl groups on the intervening phenylene linker eliminates the electronic coupling between the PTZ and AQ moieties in **PTZ-PhMe-AQ**.[78] Moreover, we show that the electron-donating ability of the PTZ moiety is also essential for the observation of the charge transfer (CT) absorption band because upon oxidation of the PTZ moiety, such a CT absorption band disappears for **O-PTZ-Ph-AQ** (Figure 2a).

The fluorescence spectra of the compounds are studied (Figure 2c). **PTZ-Ph-AQ** shows a relatively strong emission band centered at 579 nm, whereas **PTZ-PhMe-AQ** and **PTZ-Ph$_2$Me-AQ** show much weaker fluorescence. Moreover, the fluorescence of **PTZ-Ph$_2$Me-AQ** is blue-shifted at 519 nm. The stronger electronic coupling in **PTZ-Ph-AQ** makes the ^{1}CS state more emissive than the other compounds (Figure 2c). The larger distance between the PTZ and AQ units in **PTZ-Ph$_2$Me-AQ** increases the CS state energy (see a later section), leading to blue-shifted fluorescence emission. At 77 K (in frozen solution), no CT emission bands are observed, probably because either the CT is inhibited or the electronic coupling between the donor and acceptor is reduced at low temperature.[82]

We also studied the emission of the dyads under N_2 and air atmosphere (Figure 3a−c). In CHX, the emission intensity of **PTZ-Ph-AQ** is substantially quenched in aerated solution as compared to deaerated solution (Figure 3a). One possible reason is that a triplet state is involved in the emission process such as in TADF. We monitored the decay trace of the fluorescence (Figure 3d), which shows a distinct biexponential behavior in deaerated solution, with a prompt fluorescence lifetime of 62.0 ns (population ratio: 99.2%) and a delayed fluorescence component with a lifetime of 7.6 μs (0.8%). Using the exponential amplitudes and decay times, we calculated $\Phi_{DF}/\Phi_{PF} \approx 1.0$ in CHX.[54] This is an interesting result since it was previously reported that the analogue dyad without the intervening phenylene linker has no TADF properties in solution,[74,75] and its fluorescence lifetime is shorter than 0.2 ns.[75] We propose that the intervening phenylene linker in **PTZ-Ph-AQ** increases the energy of the CS state, determining a similar energy for three states (^{1}CS, ^{3}CS, and ^{3}LE). On the contrary, in the previously reported analogue **PTZ-AQ**, the CS state has a lower energy (1.9 eV) than the ^{3}AQ* state (2.7 eV), making it impossible to observe TADF, although the ^{3}CS state is populated, as confirmed by nanosecond transient absorption spectroscopy.[75] These results show that a subtle variation of the molecular structure, even the linker, may impose a significant effect on the photophysical properties of electron donor−acceptor dyads. This is also solid experimental evidence that having ^{1}CS, ^{3}CS, and ^{3}LE states sharing similar energy is essential for TADF since the ^{3}CS → ^{1}CS process is too slow to produce any TADF.[41] Moreover, it should be noted that the prompt fluorescence lifetime of **PTZ-Ph-AQ**, 62

https://doi.org/10.1021/acs.jpcb.3c02723
J. Phys. Chem. B XXXX, XXX, XXX−XXX

Table 1. Photophysical Properties of Compounds

	λ_{abs}[a] [nm]	ε[b]	λ_{em}[c] [nm]	Φ_F[d] [%]	τ_F[e]	Φ_Δ[f] [%]	τ_T[g] [μs]	V_{DA}[h] [eV]
PTZ-Ph-AQ	322[i]	1.48[i]	579	6.9	62.0 ns (99.2%)	20.1	7.0 (94.3%)	0.03
	418[j]	0.25[j]			7.6 μs (0.8%)		41.4 (5.7%)	
PTZ-PhMe-AQ	323[i]	1.50[i]	589	1.3	245.0 ns (93.5%)	10.5	1.3	0.02
					2.4 μs (6.5%)			
PTZ-Ph$_2$Me-AQ	323[i]	1.44[i]	519	1.0	3.9 ns (61.5%)	31.2	1.8 (94.6%)	0.17
					13.4 ns (38.5%)		20.3 (5.4%)	
O-PTZ-Ph-AQ	335[i]	1.24[i]	[k]	[k]	1.3 ns (93.0%)	[k]	4.2 (88.2%)	[k]
					22.9 ns (7.0%)		200.2 (11.8%)	
O-PTZ-PhMe-AQ	334[i]	1.13[i]	[k]	[k]	1.1 ns (95.9%)	[k]	47.2 (59.2%)	[k]
					20.7 ns (4.1%)		639.9 (40.8%)	
O-PTZ-Ph$_2$Me-AQ	335[i]	2.04[i]	[k]	[k]	1.5 ns (92.3%)	[k]	12.7 (65.6%)	[k]
					26.7 ns (7.7%)		1000.6 (34.4%)	
AQ	319[i]	0.51[i]	400	0.8	1.5 ns (80.8%)	68.8	36.0 (69.2%)	
					5.4 ns (19.2%)		297.8 (30.8%)	
Br-PhMe-AQ	325[i]	0.76[i]	372	0.3	0.8 ns (79.7%)	69.3	12.9 (84.1%)	
					5.9 ns (20.3%)		213.8(15.9%)	
Ph-AQ	337[i]	0.72[i]	372	0.4	0.8 ns (42.1%)	2.0	16.0(88.4%)	
					5.2 ns (57.9%)		332.3(11.6%)	

[a]Maximal UV−vis absorption intensity wavelength in CHX (1.0×10^{-5} M). [b]Molar absorption coefficient at the absorption maxima, $\varepsilon = 10^4$ M^{-1} cm^{-1}. [c]Maximal fluorescence intensity wavelength in CHX. [d]Absolute fluorescence quantum yields, determined with an optical integration sphere. [e]Fluorescence lifetime in CHX under N_2 (λ_{ex} = 340 nm). [f]Singlet oxygen quantum yield ($^1O_2$) with Ru(bpy)$_3$[PF$_6$]$_2$ as standard (Φ_Δ = 57% in DCM) in CHX. [g]Triplet state lifetime in CHX determined with nanosecond transient absorption spectra. [h]Electronic coupling matrix element of the excited state, calculated by CT emission in CHX. [i]The absorption of the ^{1}LE state. [j]The absorption of the ^{1}CT state. [k]Not observed.

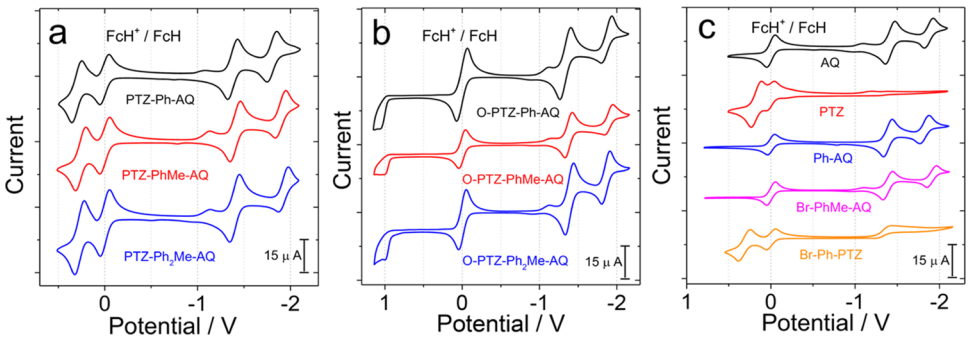

Figure 4. Cyclic voltammogram of the compounds. Ferrocene (FcH/FcH$^+$) was used as an internal reference. Condition: in deaerated DCM containing 0.10 M $Bu_4N[PF_6]$ as a supporting electrode and Ag/AgNO$_3$ as a reference electrode. Scan rates: 100 mV/s. $c = 1.0 \times 10^{-3}$ M, 20 °C.

ns, is exceptionally long for electron donor−acceptor type TADF emitters.[43,44,83] Note that the E_{T1} of the 2-phenylanthraquinone is 2.33 eV,[77] and for the native AQ, the T_1 state energy is ca. 2.7 eV,[84] while the CS state energy of **PTZ-Ph-AQ** is ca. 2.49 eV based on the electrochemical studies. Interestingly, since the PTZ moiety has a T_1 state energy of 2.6 eV, **PTZ-Ph-AQ** is a unique example among TADF compounds, where two ^{3}LE states share similar energy with the emissive CS state.

In HEX, a solvent with slightly higher polarity than CHX ($E_T(30)$ values of CHX and HEX are 30.9 and 31.0 kcal mol^{-1}, respectively), the luminescence lifetimes were determined as 53.4 ns (99.7%)/3.4 μs (0.3%) (Figure 3e). The CS state energy of **PTZ-Ph-AQ** is lower in HEX than that in CHX, and the smaller energy gap between the ^{3}CS and ^{3}AQ* state makes the delayed fluorescence an efficient drain channel for the excited state, shortening the lifetime. In TOL ($E_T(30)$ = 33.9 kcal mol^{-1}), the fluorescence lifetime is even shorter (Figure 3f), and no delayed fluorescence was observed. We propose that the $E_T(30)$ parameter is more appropriate than the permittivity under this circumstance. The permittivity of the solvents are ε_{HEX} = 1.88, ε_{CHX} = 2.02, and ε_{TOL} = 2.38.

We then studied the effect of the conformation restriction on TADF. For **PTZ-PhMe-AQ**, with methyl groups attached on the phenylene linker, the prompt fluorescence lifetime is 245 ns (93.5%), the delayed fluorescence lifetime is reduced to 2.4 μs, and the percentage is 6.5% (Figure S29) as compared to **PTZ-Ph-AQ**. Using the exponential amplitudes and decay times calculated $\Phi_{DF}/\Phi_{PF} \approx 0.7$ in CHX, a similar value is compared to **PTZ-Ph-AQ** ($\Phi_{DF}/\Phi_{PF} \approx 1.0$).[54] It should be pointed out that such a long-lived prompt fluorescence in electron donor−acceptor type of TADF emitters is very rare,[85] and only recently, we reported an exceptionally long-lived prompt fluorescence lifetime for an AQ-PhMe-phenoxazine dyad (282 ns).[81] This long prompt fluorescence lifetime is attributed to the weak coupling between the radical anion and cation in the CS state, which makes the CS state weakly emissive. Note that the CT emission band of **PTZ-PhMe-AQ** is centered at 589 nm, which is slightly red-shifted as compared to that of **PTZ-Ph-AQ** (579 nm): this can be explained by the conformation restriction. The ^{3}AQ* state energy of **PTZ-**

https://doi.org/10.1021/acs.jpcb.3c02723
J. Phys. Chem. B XXXX, XXX, XXX−XXX

Table 2. Electrochemical Redox Potentials, Driving Forces of Charge Separation (ΔG_{CS}), and the Energy of the Charge-Separated State (E_{CS}) of the Compounds in Different Solvents[a,d,e]

			ΔG_{CS}/eV					E_{CS}/eV				
	E_{ox}[f]/V	E_{red}[f]/V	HEX	CHX	TOL	DCM	ACN	HEX	CHX	TOL	DCM	ACN
PTZ-Ph-AQ[b]	+0.30	−1.38, −1.80	−0.46	−0.57	−0.74	−1.53	−1.75	2.60	2.49	2.32	1.53	1.31
PTZ-PhMe-AQ[b]	+0.26	−1.40, −1.90	−0.48	−0.59	−0.76	−1.55	−1.77	2.58	2.47	2.30	1.51	1.29
PTZ-Ph$_2$Me-AQ[b]	+0.27	−1.40, −1.93	−0.28	−0.40	−0.60	−1.50	−1.75	2.78	2.66	2.46	1.56	1.31
O-PTZ-Ph-AQ[c]	+1.06	−1.34, −1.88	0.13	0.04	−0.14	−0.91	−1.12	3.29	3.20	3.02	2.25	2.04
O-PTZ-PhMe-AQ[c]	+1.02	−1.37, −1.89	0.15	0.06	−0.13	−0.92	−1.13	3.31	3.22	3.03	2.24	2.03
O-PTZ-Ph$_2$Me-AQ[c]	+1.00	−1.39, −1.86	0.34	0.23	0.02	−0.88	−1.12	3.50	3.39	3.18	2.28	2.04

[a]Cyclic voltammetry in N_2-saturated DCM containing a 0.10 M $Bu_4N[PF_6]$ supporting electrolyte, counter electrode as the Pt electrode, working electrode as the glassy carbon electrode, and $Ag/AgNO_3$ couple as the reference electrode. E_{00} (E_{00} = 1240/λ) is the singlet state energy of compounds,. [b]λ is approximated from an average value between absorption and emission in CHX. [c]λ is approximated from an average value between absorption and emission of AQ in CHX. [d]E_{00} = 3.06 eV. [e]E_{00} = 3.16 eV. [f]The value is obtained by setting the oxidation wave of FcH/FcH$^+$ as 0 V.

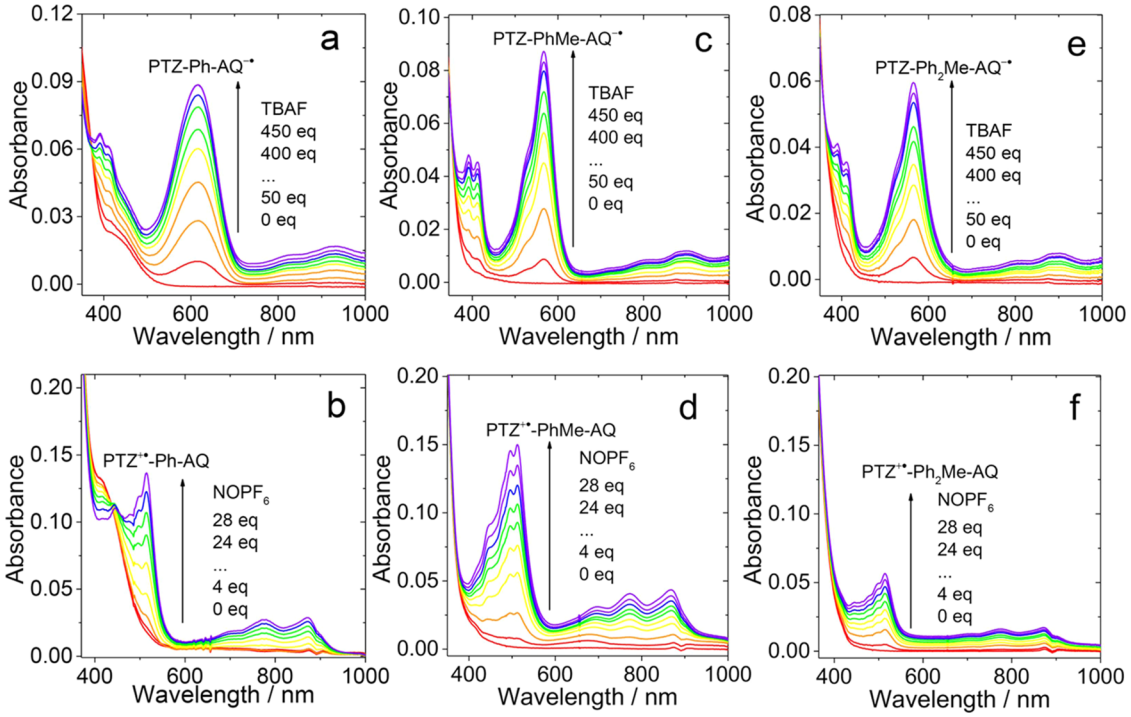

Figure 5. Evolution of the UV−vis absorption spectra of (a) **PTZ-Ph-AQ**, (c) **PTZ-PhMe-AQ**, and (e) **PTZ-Ph$_2$Me-AQ** in the presence of increasing amount of tetra-*n*-butylammonium fluoride (TBAF) as a reductant. $c = 5.0 \times 10^{-5}$ M, in deaerated DMF, 20 °C. Evolution of the UV−vis absorption spectra of (b) **PTZ-Ph-AQ**, (d) **PTZ-PhMe-AQ**, and (f) **PTZ-Ph$_2$Me-AQ** in the presence of increasing nitrosonium hexafluorophosphate ($NOPF_6$) as an oxidant. $c = 5.0 \times 10^{-5}$ M, in dry and deaerated ACN, 20 °C.

PhMe-AQ is 2.74 eV based on the phosphorescence (Figure S32), which is slightly higher than the CS state energy (2.47 eV) based on the electrochemistry.

For **PTZ-Ph$_2$Me-AQ**, interestingly, no significant TADF was observed (Figure S29), although the fluorescence decay traces show a biexponential character (Table 1). With increasing the distance between the donor and the acceptor in the dyads, the CS state energy should increase as compared to that of **PTZ-PhMe-AQ**.[82] This is demonstrated by the CT emission bands of **PTZ-Ph$_2$Me-AQ**, which are centered at 517 nm, 506 nm, and 611 nm in CHX, HEX, and TOL, respectively. In comparison, the corresponding CT emission bands of **PTZ-PhMe-AQ** are at 589, 579, and 692 nm, respectively. For **PTZ-Ph$_2$Me-AQ**, the CS state energy is ca. 2.66 eV based on the electrochemistry. In comparison, **Br-PhMe-AQ** has a T_1 state energy of 2.74 eV.

3.3. Electrochemical Characterization and the Absorption Spectra of the Radical Anion and Cation of the Dyads. The redox properties of the dyads and reference compounds were studied by cyclic voltammetry (Figure 4a,b,c). For **PTZ**, a reversible oxidation wave at +0.18 V (vs FcH/FcH$^+$) was observed, whereas for **AQ**, two reversible reduction waves at −1.42 and −1.87 V were observed (Figure 4c).

For the dyad **PTZ-Ph-AQ**, one reversible oxidation wave at +0.30 V (vs FcH/FcH$^+$) was observed, differently from the native **PTZ** (+0.18 V). Moreover, two reversible reduction waves at −1.38 and −1.80 V were observed, which are different from the native **AQ** (−1.42 and −1.87 V). For **Ph-AQ**, two reversible reduction waves at −1.39 and −1.82 V were observed. These results confirm the electronic interaction between the AQ and PTZ units in **PTZ-Ph-AQ** at the ground

https://doi.org/10.1021/acs.jpcb.3c02723
J. Phys. Chem. B XXXX, XXX, XXX−XXX

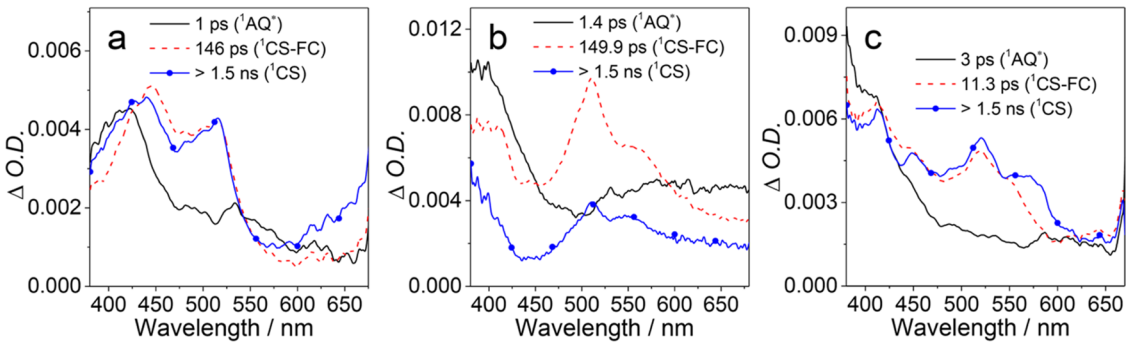

Figure 6. EADS obtained from global analysis of the transient absorption data measured in CHX for (a) **PTZ-Ph-AQ**, (b) **PTZ-PhMe-AQ**, and (c) **PTZ-Ph$_2$Me-AQ**. "FC" stands for Franck−Condon.

state. For the analogous dyad with methyl groups attached on the phenylene linker, the redox potentials are slightly different from that of **PTZ-Ph-AQ**. Induction effect is possible, supported by the redox potential of the dyads with the PTZ unit oxidized, generally, the reduction potentials are cathodically shifted. The Gibbs free energy changes of the electron transfer (ΔG_{CS}) in the dyads in solvents with different polarities were studied (see the Supporting Information for details). The ΔG_{CS} values are all negative in solvents with different polarities for the dyads containing the PTZ unit (Table 2). These results suggest the occurrence of CS, in agreement with the fluorescence studies. For the dyads with the PTZ unit oxidized, however, the ΔG_{CS} values of **O-PTZ-Ph-AQ** and **O-PTZ-PhMe-AQ** are negative in TOL, DCM, and acetonitrile (ACN), and the ΔG_{CS} value of **O-PTZ-Ph$_2$Me-AQ** is negative in DCM and ACN (Table 2).

The CS state energy was also calculated based on the electrochemical and spectral data (Table 2). The results show that the energy of the CS state is higher compared to the previously reported analogue without the intervening phenylene linker (ca. 2.0 eV).[75] Moreover, the CS state energy becomes lower in solvents with higher polarity. For instance, the CS state energies of **PTZ-Ph-AQ** are 2.60, 2.49, 2.32, 1.53, and 1.31 eV in CHX, HEX, TOL, DCM, and ACN, respectively. A similar trend was observed for other dyads (Table 2). Since the ^{3}LE states (here, it is ^{3}AQ* and ^{3}PTZ*) are less dependent on the solvent polarity, we can expect a substantial solvent effect on the photophysical properties of the dyads, especially on the TADF emission. With a longer linker between the donor and acceptor, thus the larger distance between the donor and acceptor, the CS state energy becomes higher. For instance, the energy of the CS state of **PTZ-Ph$_2$Me-AQ** is generally higher than that of **PTZ-PhMe-AQ** (Table 2). The ^{3}AQ* state energy is known as 2.7 eV.[84] The pristine PTZ has a similar T_1 state energy of ca. 2.6 eV.[84] Based on the calculated CS state energy, the ^{3}AQ* state and CS states have similar energy in nonpolar solvents, but in polar solvents, the CS state becomes much lower in energy. This is confirmed by the nanosecond transient absorption spectral studies (see a later section).

To aid the assignment of the CS states of the dyads in transient absorption spectra, we analyzed UV−vis absorption spectra of the anion and the cation units using chemical reduction or oxidation (Figure 5). For **PTZ-Ph-AQ**, the absorption band of the radical anion AQ$^{-\bullet}$ centered at 616 nm was observed upon addition of the reductant Bu_4NF,[86] together with minor absorption bands in the region of 700−1000 nm (Figure 5a), similarly to the previously reported analogues PTZ-AQ containing a rigid bicyclo[2.2.2]octane linker.[77,87] For **PTZ-PhMe-AQ**, the absorption band of AQ$^{-\bullet}$ is centered at 567 nm (Figure 5c), blue-shifted by 49 nm as compared to that of **PTZ-Ph-AQ**. This result can be attributed to the conformation restriction and the interrupted π-conjugation between the AQ and the phenylene units. The anion absorption spectra of **AQ** are similar to those of **PTZ-PhMe-AQ** (Figure S34). Similar results were observed for **PTZ-Ph$_2$Me-AQ** (Figure 5e).

The absorption bands of the PTZ$^{+\bullet}$ of three compounds were obtained by mixing the oxidant $NOPF_6$ with the dyads (Figure 5b,d,f). We observed absorption bands of PTZ$^{+\bullet}$ at 510 nm and in the range of 600−950 nm, similar for three compounds. However, the absorption bands observed for photoinduced CS states are different from those of radical anion or cation obtained through chemical oxidation or reduction (see also the spectroelectrochemistry studies, Figure S33). Indeed, upon photoexcitation, both the radical anion and cation coexist in the CS state, with possible electronic interaction between the radical cation and anion, whereas using chemical reduction or oxidation, separated D−A$^{-\bullet}$ or D$^{+\bullet}$−A is formed, with no interaction between the anion and the cation.

3.4. Femtosecond Transient Absorption (fs-TA) Spectroscopy. The excited state relaxation of the compounds was analyzed by means of transient absorption spectroscopy with fs time resolution. The transient absorption spectra of the compounds were recorded both in CHX and ACN in order to investigate the effect of solvent polarity on their excited state dynamics. Global analysis of the recorded kinetic traces was employed for obtaining the kinetic constants accounting for the dynamics of excited state relaxation (Figure 6). In all cases, we used a linear unidirectional decay scheme, giving the evolution associated difference spectra (EADS) associated with each kinetic constant.[88] To assign the transient bands observed for bichromophoric compounds, we preliminary measured the transient spectra of the reference compounds **Br-PhMe-AQ** and **Ph-AQ** (Figure S35). For **Br-PhMe-AQ**, the transient spectrum at short timescale shows the appearance of an excited state absorption (ESA) band peaked at about 380 nm, assigned to the S_1 state of the AQ compound. Because of the presence of the heavy atom, the system undergoes rapid ISC, in about 2.2 ps, toward the ^{3}AQ* state, characterized again by an ESA band peaked at about 380 nm, more intense than that observed for the singlet state, and a second, very broad band in the 600 nm region. For **Ph-AQ**, the initially observed ESA band, assigned to the singlet excited state, peaks at 430 nm, red-shifted compared to the **Br-PhMe-AQ**. Furthermore, within

https://doi.org/10.1021/acs.jpcb.3c02723
J. Phys. Chem. B XXXX, XXX, XXX−XXX

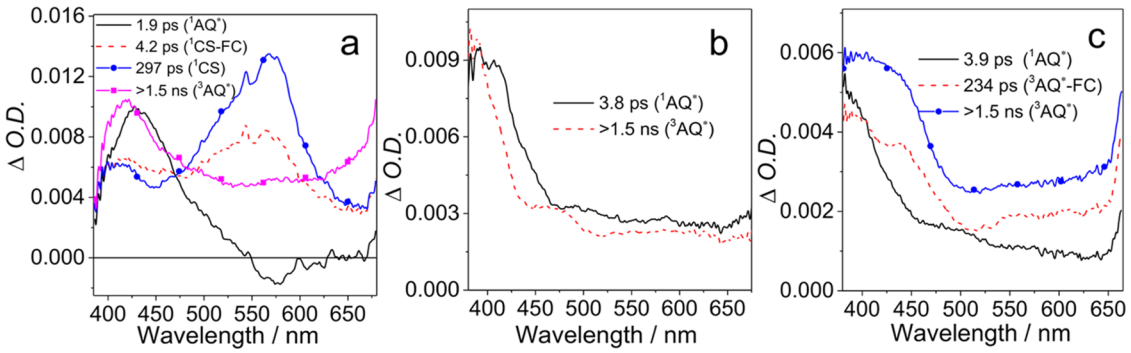

Figure 7. EADS obtained from global analysis of the transient absorption data measured in CHX for (a) **O-PTZ-Ph-AQ**, (b) **O-PTZ-PhMe-AQ**, and (c) **O-PTZ-Ph$_2$Me-AQ**.

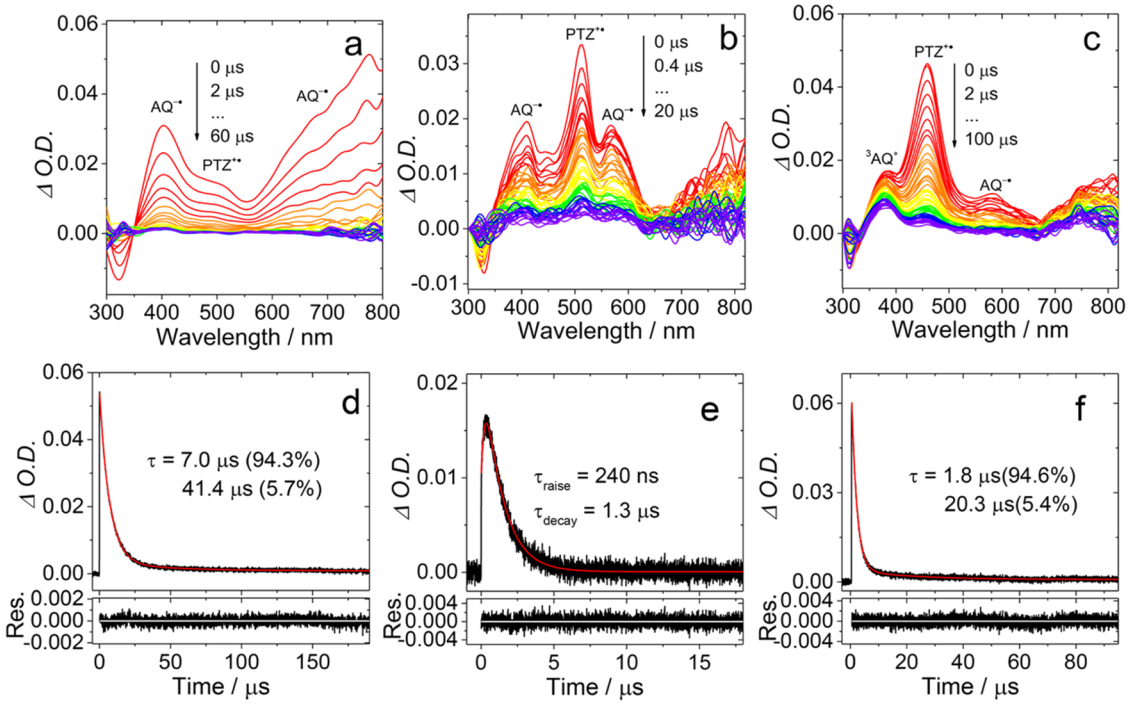

Figure 8. Nanosecond transient absorption spectra of (a) **PTZ-Ph-AQ**, (b) **PTZ-PhMe-AQ**, and (c) **PTZ-Ph$_2$Me-AQ** at different delay time. Decay traces of (d) **PTZ-Ph-AQ** at 400 nm, (e) **PTZ-PhMe-AQ** at 570 nm, (f) **PTZ-Ph$_2$Me-AQ** at 460 nm. λ_{ex} = 355 nm, $c = 3.0 \times 10^{-5}$ M in deaerated CHX, 20 °C.

about 2 ps, a weak band centered at 400 nm and an intense band centered at 572 nm are developed, suggesting the formation of the ^{3}AQ* state. The ^{3}AQ* state does not decay on the timescale of the experiment.[77,89]

The EADS obtained by global analysis of the transient data acquired for the compounds **PTZ-Ph-AQ**, **PTZ-PhMe-AQ**, and **PTZ-Ph$_2$Me-AQ** are presented in Figure 6. In the case of **PTZ-Ph-AQ**, the initial EADS show the appearance of an ESA band peaked at about 430 nm (Figure 6a), with a broad tail extending on the red part of the spectrum, which can be assigned as the singlet excited state localized on the AQ moiety, by comparison with the reference compounds. In about 1 ps, the spectrum evolves toward the second EADS, presenting two intense ESA bands, respectively, peaked at 445 and 520 nm. The comparison with the spectra of anion and cation species reported in Figure 5 allows us to interpret these bands, respectively, due to PTZ$^{+\bullet}$ and AQ$^{-\bullet}$, thus demonstrating the occurrence of fast CS even in the nonpolar solvent CHX. On the following 146 ps timescale, we observe a small spectral evolution: the 445 nm band slightly blue shifts and a broad absorption band at wavelengths >600 nm develops. The final spectral component lives well behind the time interval explored with the measurement (1.5 ns). The development of the broad ESA band at >600 nm and the long lifetime of the last spectral component suggest that the state reached at about 150 ps could be a ^{3}CS state. In ACN, we also observe the formation of a CS state on a faster 0.7 ps timescale. In this case, however, the transient signal mostly recovers on a fast 5.4 ps timescale, leaving a small intensity residual signal still assigned as the singlet CS state of the system. The different dynamics observed in the two solvents can be inferred by the comparison of the kinetic traces recorded on the maximum of the AQ$^{-\bullet}$ absorption band (Figure S38).

CS occurs on a fast timescale in CHX also for the other two compounds **PTZ-PhMe-AQ** (Figure 6b) and **PTZ-Ph$_2$Me-AQ** (Figure 6c), as noticed by examining the EADS. More in detail, peaks assignable to PTZ$^{+\bullet}$ and AQ$^{-\bullet}$ are observed in the second EADS (red trace) for both compounds, which develop

https://doi.org/10.1021/acs.jpcb.3c02723
J. Phys. Chem. B XXXX, XXX, XXX−XXX

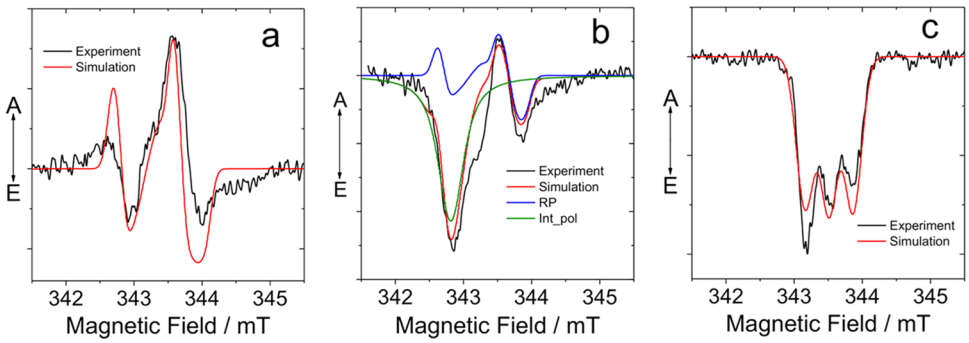

Figure 9. TREPR spectra of the dyads in toluene at room temperature at 9.63 GHz (X-band spectrometer): (a) **PTZ-Ph-AQ**, (b) **PTZ-PhMe-AQ**, and (c) **PTZ-Ph$_2$Me-AQ**. The red lines are the simulation.

in about 1.4 ps and 3 ps, respectively. In the case of **PTZ-PhMe-AQ**, the transient signal partially decays in about 150 ps, while for **PTZ-Ph$_2$Me-AQ**, a relaxation process of the CS state occurs in about 11 ps. The limited spectral difference between the second and third EADS suggests the long-living species being the singlet CS state for both compounds, whose lifetime is >1.5 ns. Note that with increasing of the distance, the CS process becomes slower, which can be attributed to the decreased driving force, although the increasing distance between the donor and acceptor may affect the reorganization energy, causing in some case an anti-intuitive faster CS with increasing the distance.[76] CS occurs in about 1−2 ps in ACN, where a fast decay component is observed, as detected for **PTZ-Ph-AQ**, also for **PTZ-PhMe-AQ** and **PTZ-Ph$_2$Me-AQ** (Figure S38d−f).

We furthermore acquired the transient absorption spectra of analogous compounds containing an oxidized PTZ, whose EADS in CHX are presented in Figure 7. In the case of **O-PTZ-Ph-AQ**, the initial spectral component (Figure 7a), living 1.9 ps, is assigned as the S_1 state of the system, mostly localized on the AQ moiety. The development of an intense band peaked at about 570 nm in the second EADS suggests the formation of a CS state. The intensity of the 570 nm band further increases on the following 4.2 ps timescale. The transient spectral shape notably evolves on the following 297 ps timescale: the 570 nm band recovers, indicating the occurrence of charge recombination, while an ESA band peaked at about 430 nm with an intense broad tail develops. By comparison with the reference compounds, we assign the final EADS as the triplet state localized on the AQ moiety, as also observed on the longer ns timescale (see next paragraph). CS does not occur in CHX in the case of **O-PTZ-PhMe-AQ**: (looking at the EADS reported in Figure 7b), it appears that the system remains in an excited state localized on the AQ moiety, presenting a long lifetime. For **O-PTZ-Ph$_2$Me-AQ**, we observe the development of a band peaked at 450 nm in the second EADS (Figure 7c), attributed to the unrelaxed ^{3}AQ* state, suggesting the occurrence of ISC in 3.9 ps. The spectral shape of the final EADS is reminiscent of the ^{3}AQ* state. For all of the three compounds, CS was observed in ACN (Figure S37).

3.5. Nanosecond Transient Absorption (ns-TA) Spectroscopy. To study the long-living transient species formed in the dyads upon photoexcitation, the ns-TA spectra of the compounds upon pulsed laser photoexcitation were recorded. First, the reference compounds were studied. For **AQ** and **Br-PhMe-AQ**, an ESA band centered at 380 nm was observed (Figure S39), attributed to the ^{3}AQ* state. For **Ph-AQ**, we observed ESA bands centered at 400 nm and 580 nm (Figure S41), which are attributed to the ^{3}AQ* state, supported by previous reports.[77] The triplet state of PTZ is characterized by an absorption band at 460 nm, with a molecular absorption coefficient of 27,000 M^{-1} cm^{-1}.[84]

For **PTZ-Ph-AQ**, a strong positive absorption band centered at 400 nm was observed (Figure 8a), attributed to $AQ^{-\bullet}$, as well as a weak positive absorption band centered at 510 nm, attributed to $PTZ^{+\bullet}$. A broad absorption band in the range of 600−800 nm was also observed, which is tentatively assigned to $AQ^{-\bullet}$. The lifetime of the transient species was determined as 7.0 μs, in good agreement with the delayed fluorescence lifetime (7.6 μs. Figure 3d). The component with longer lifetime of 41.4 μs may be due to intermolecular charge recombination.

For **PTZ-PhMe-AQ**, different transient absorption features were observed (Figure 8b). The spectra show positive absorption bands centered at 410, 510, and 570 nm, which are attributed to the $AQ^{-\bullet}$ radical anion (410 and 570 nm) and the $PTZ^{+\bullet}$ radical cation (510 nm), respectively, demonstrating also in this case the formation of a CS state. Interestingly, the kinetic traces show a growth and a decay phase, with the rise taking 240 ns (the IRF of the spectrometer is ca. 7 ns) and the decay taking 1.3 μs. These times are similar to the measured luminescence lifetimes, 245 ns for the prompt fluorescence and 2.4 μs for the delayed fluorescence (Figure S29). We attribute the rise component to the depletion of the ^{1}CS state, which causes an apparent bleaching band centered at 600 nm due to its emissive feature. Thus, the ^{1}CS state lifetime is ca. 240 ns, and the final ^{3}CS state has a lifetime of 1.3 μs.[81] Note, in this case, we cannot confirm whether or not there is ^{1}CS → ^{3}CS process, i.e., we cannot discriminate the scenario in which ^{1}CS and ^{3}CS are formed simultaneously or there is a ^{1}CS → ^{3}CS process following the formation of the ^{1}CS state. The discrepancy between the ^{3}CS state lifetime determined with the ns-TA and TADF fluorescence study is due to the different excitation power and the more significant triplet−triplet annihilation (TTA) self-quenching effect in the ns-TA spectral measurements. For **PTZ-Ph$_2$Me-AQ** in CHX (Figure 8c), the ns-TA spectra show positive absorption bands centered at 460 and 580 nm, which are attributed to the absorption of $PTZ^{+\bullet}$ (460 nm) and $AQ^{-\bullet}$ (580 nm), respectively. Another feature of the CS states observed for **PTZ-PhMe-AQ** and **PTZ-Ph$_2$Me-AQ** is that the relative intensity of the absorption bands of the anion and cation is different from the previously reported PTZ-AQ dyads, which is probably due to the conformation restriction (Figure 8).

https://doi.org/10.1021/acs.jpcb.3c02723
J. Phys. Chem. B XXXX, XXX, XXX−XXX

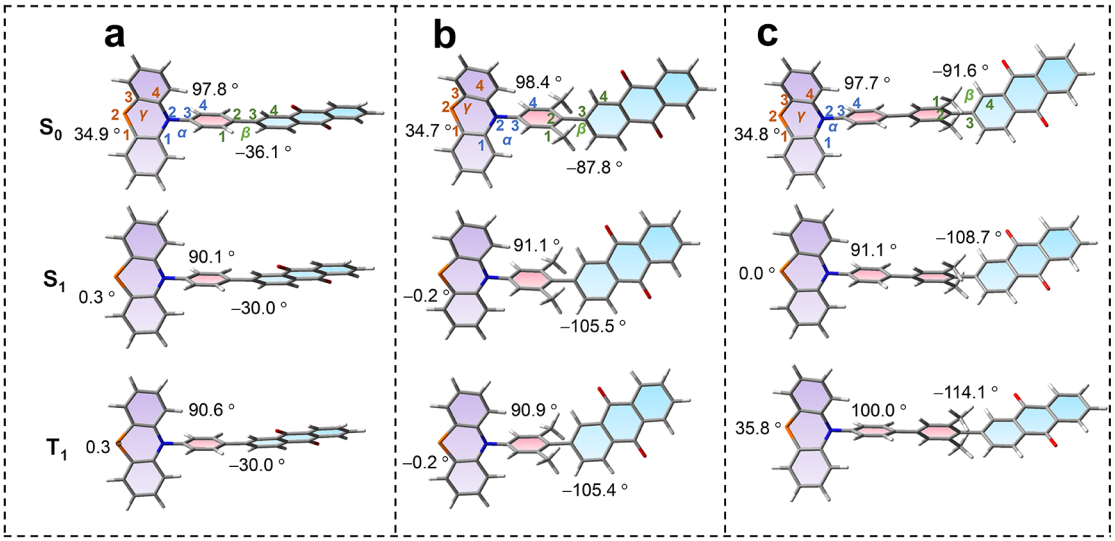

Figure 10. Optimized conformations and labeling of the torsion angles between the donor and the acceptor of the selected atoms of the ground state (top row) in vacuum, the S_1 state (middle row), and the T_1 state (bottom row) of (a) **PTZ-Ph-AQ**, (b) **PTZ-PhMe-AQ**, and (c) **PTZ-Ph$_2$Me-AQ** in CHX.

The ns-TA spectra of the dyads in a polar solvent such as ACN were also measured. For **PTZ-Ph-AQ**, a CS state was observed, with a lifetime of ca. 100 ns (Figure S46). Based on the lifetime, we attribute it to a ^{3}CS state. The shorter lifetime in ACN as compared to that in CHX can be attributed to the energy gap law because the CS state has a much lower energy of 1.31 eV in ACN compared to CHX (2.49 eV).[21,90] For **PTZ-PhMe-AQ**, we observed a CS state, whose lifetime is shortened to 440 ns, as compared to 1.3 μs in CHX. The longer CS state lifetime of **PTZ-PhMe-AQ** compared to **PTZ-Ph-AQ** is attributed to the weak electronic coupling between the donor and acceptor. For **PTZ-Ph$_2$Me-AQ**, the CS lifetime in ACN is 1.3 μs, similar to that in CHX (1.8 μs). The longer CS state lifetime of **PTZ-Ph$_2$Me-AQ** is attributed to the weaker electronic coupling between the electron donor and acceptor. We furthermore acquired the transient absorption spectra of analogous compounds containing an oxidized PTZ; for these compounds, we always observed the signatures of the ^{3}AQ* state (Figure S48).

3.6. Time-Resolved Electron Paramagnetic Resonance (TREPR) Spectral Study. In order to quantitatively describe the CS state formed in the dyads upon photoexcitation, the pulsed laser-excited TREPR spectra of the compounds in fluid solution at room temperature were recorded (Figure 9). From the polarization pattern of the TREPR spectra and the simulation, the electron spin−spin dipolar interaction magnitude and the electron exchange interaction (both sign and magnitude) can be obtained.[3,91−93] The polarization phase pattern of the TREPR spectra of radical ion pair (RIP) is dependent on the sign and magnitude of the electron exchange energy (J) and the spin multiplicity of the precursor of the charge separation process.[3]

For **PTZ-Ph-AQ** (Figure 9a), an A, E, A, E antiphase spectrum was observed, which is a typical feature of spin-correlated radical pair (SCRP).[91,94,95] Simulation of the spectrum gives an electron exchange value of $2J$ = +60 MHz (2.14 mT). The polarization pattern and the positive sign of the J value indicate that the CS state has a triplet precursor.[3] This is in agreement with the optical spectral studies. Previously, a phenothiazine trimer-AQ containing bicyclo[2.2.2]octane linker showed a SCRP spectrum, however, J = +0.8±0.2 mT ($H = -2J$ **S1S2**), and an opposite polarization pattern was observed.[95] The slightly large J magnitude in our case is reasonable because the linker in **PTZ-Ph-AQ** is shorter. In a triphenylamine−nathphalenediimide dyad based on an N^N Pt(II) bisacetylide framework, an SCRP signal with A, E, A, E, A, E was observed, and the J was determined as +0.05 mT.[94] For **PTZ-PhMe-AQ**, different spectra were observed, but simulation indicates that a similar A,E polarized SCRP species and a species with net (integrated) emissive polarization exist (Figure 9b). For **PTZ-Ph$_2$Me-AQ**, interestingly, an all-emissive signal was observed (Figure 9c). Simulation gives $|2J| \geq 8A(^{14}N)$, i.e., 184 MHz (6.57 mT). Note that the electron exchange interaction in this dyad is stronger than that of **PTZ-PhMe-AQ** and **PTZ-Ph-AQ**, although the linker in **PTZ-Ph$_2$Me-AQ** is longer. Previously, an emissive TREPR spectrum was observed for the PTZ-AQ dyad with the bicyclo[2.2.2]octane linker, for which $|J|$ > 1.5 mT.[95] In an analogue, a similar emissive TREPR spectrum was observed, and $|J|$ = 1.5−2.2 mT was found.[77] Note that the relationship between the electron exchange magnitude and sign and spectral observable parameters is complicated and it is not straightforward to correlate both easily. However, these results unambiguously demonstrated that the electron exchange interaction of the CS states is generally in a weak interaction regime.[30,31,34,50,59,96]

3.7. Computational Explanation of the Different Emission Properties of the Dyads. The ground-state S_0 geometry of the dyads was optimized at the B3LYP/6-31G* level of theory. For **PTZ-Ph-AQ**, the dihedral angle α between the PTZ and the intervening phenylene linker and the dihedral angle β between the phenylene linker and the AQ unit are 978 and −36.1°, respectively. In comparison, the corresponding dihedral angles in **PTZ-PhMe-AQ** are 98.4 and −87.8°, respectively. The larger dihedral angle between the phenylene linker and AQ in **PTZ-PhMe-AQ** is due to the conformational restriction effect imposed by the methyl groups on the linker. For **PTZ-Ph$_2$Me-AQ**, similar dihedral angles were observed. Interestingly, for all three compounds, in the ground state S_0, the PTZ unit adopts a puckered geometry, with a computed

https://doi.org/10.1021/acs.jpcb.3c02723
J. Phys. Chem. B XXXX, XXX, XXX−XXX

Table 3. Calculated Photophysical Data for the Three Investigated Dyads, Reporting the Vertical Excitation Energies (in eV and nm) with Their Corresponding Assignment of the Excited from One-Electron TDA−DFT Excitations, Oscillator Strength (f), and Main Configurations; Computed S−T Gaps (eV) Along with SOC Values (cm^{-1}) between the ^{1}CS and ^{3}LE Involved in the ISC Process

	state[a]	energy eV/nm		main configuration	f	ΔE_{ST}^{V}	SOC(^{1}CS−^{3}LE)	ΔE(^{1}CS−^{3}LE)	ΔE(^{3}LE−^{3}CS)
PTZ-Ph-AQ	^{1}CS	2.11	587	H → L (95%)	0.0001	0.002	0.12	−0.11	0.11
	^{1}CS	3.02	410	H−2 → L (22%)	0.1417				
				H−3 → L (64%)					
	^{1}LE$_A$	3.87	321	H−8 → L (7%)	0.1258				
				H−10 → L (58%)					
				H−12 → L (9%)					
	^{3}CS	2.11	588	H → L (95%)					
	^{3}LE$_A$	2.22	558	H−2 → L (72%)					
				H−3 → L (26%)					
PTZ-PhMe-AQ	^{1}CS	2.09	592	H → L (98%)	0.0002	0.0001	0.12	−0.16	0.16
	^{1}LE$_A$	3.56	348	H−11 → L (84%)	0.1676				
	^{1}LE$_D$	3.92	317	H → L+8 (85%)	0.0593				
	^{3}CS	2.09	592	H → L (98%)					
	^{3}LE$_A$	2.25	552	H−3 → L (85%)					
PTZ-Ph$_2$Me-AQ	^{1}CS	2.53	491	H → L (99%)	0.0000	0.30	0.04		
	^{3}LE$_A$	3.51	353	H−11 → L (93%)	0.1926				
	^{1}LE$_D$	3.87	321	H → L+9 (83%)	0.0708				
	^{3}LE$_A$	2.22	557	H−3 → L (93%)					
	^{3}CS	2.51	494	H−7 → L (95%)					
	^{3}CS	2.53	491	H → L (99%)					

[a]The nature of each state is based on the NTO analysis; for the LE state, the localization of the charge density on donor (D) or acceptor (A) portion is provided.

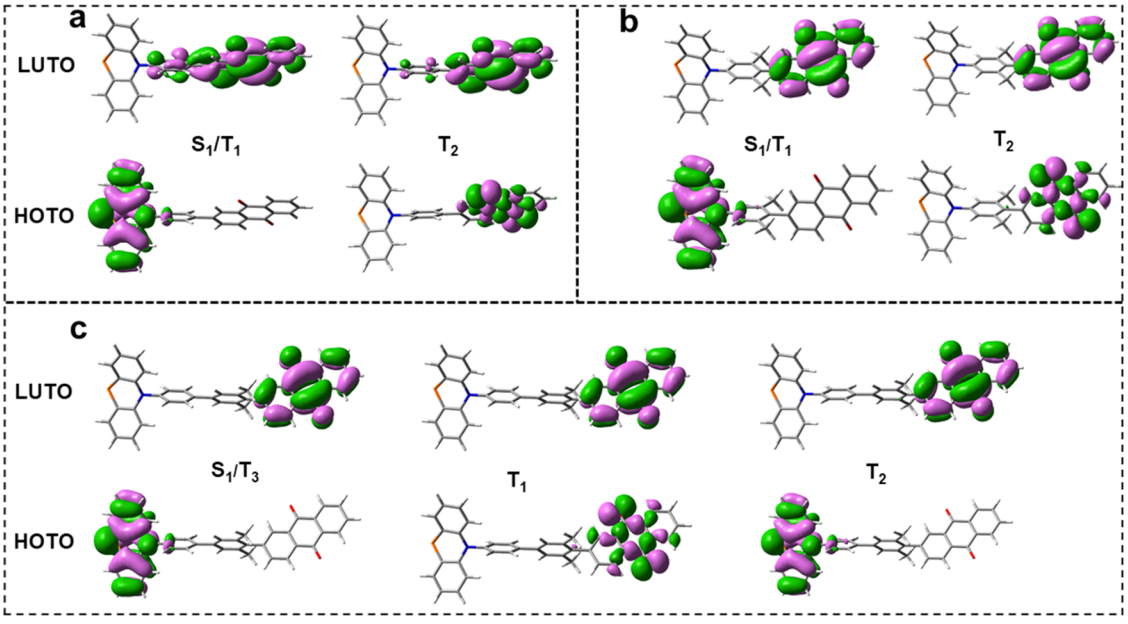

Figure 11. Highest occupied transition and lowest unoccupied transition orbitals for selected excited states of (a) **PTZ-Ph-AQ**, (b) **PTZ-PhMe-AQ**, and (c) **PTZ-Ph$_2$Me-AQ**.

dihedral angle γ between the two phenylene rings of ca. 35°. The calculated dihedral angles are presented in Figure 10.

Starting from the gas-phase optimized geometry, we have performed TD-DFT calculations within the Tamm−Dancoff approximation (TDA)[68] in CHX to evaluate the effect of the different linkers on the absorption spectra and photophysical properties. Table 3 lists the main excitation energies along with the related oscillator strengths and the character of the transitions for the three dyads. The corresponding energy difference (ΔE_{ST}) is also listed along with the computed SOC values. Our TDA−DFT calculations show that two bright states at 410 and 321 nm are calculated for the **PTZ-Ph-AQ** dyad. For the other two compounds, all of the transitions involving the singlet states below ca. 350 nm have oscillator strengths almost equal to zero, and the relevant ones are peaked at 348 and 317 nm for **PTZ-PhMe-AQ** and 353 nm and 321 nm for **PTZ-Ph$_2$Me-AQ**. These results well reproduce the two experimental adsorption bands observed at 418 and

https://doi.org/10.1021/acs.jpcb.3c02723
J. Phys. Chem. B XXXX, XXX, XXX−XXX

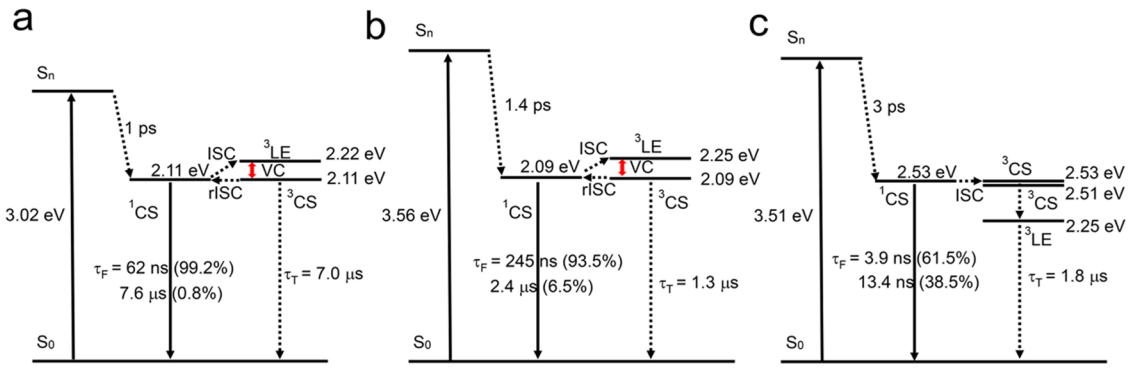

Figure 12. Simplified Jablonski diagram illustrating the photophysical processes involved in (a) **PTZ-Ph-AQ**, (b) **PTZ-PhMe-AQ**, and (c) **PTZ-Ph$_2$Me-AQ**. The energy of the singlet, CS, and triplet state are from the DFT calculation. VC stands for vibronic coupling.

322 nm for the **PTZ-Ph-AQ** compound and the lack of adsorption bands at a longer wavelength for **PTZ-PhMe-AQ** and **PTZ-Ph$_2$Me-AQ**. However, in these latter cases, the sole absorption band recorded at 323 nm is found to be originated from two different excitations cited above.

The S_1 state of the dyads was optimized in CHX, and the corresponding geometries are shown in Figure 10. At the S_1 state, the α angles of all three dyads are about 7°, smaller than the corresponding ones at the S_0 state. On the other hand, smaller values of about 17° for β are calculated for both **PTZ-PhMe-AQ** and **PTZ-Ph$_2$Me-AQ**, while a larger β of ∼6° is obtained for **PTZ-Ph-AQ**. Overall, the dihedral angles of the dyads do not show any significant changes in their S_1 states with respect to S_0, suggesting that no electronic states involve π-conjugation between different units in the dyad. Interestingly, the PTZ units adopt planar geometry in the S_1 state of the three dyads. Since it is known that the $PTZ^{+\bullet}$ radical cation adopts planar geometry, this confirms the S_1 state as a CS state. This conclusion is also supported by the analysis of the NTOs discussed below, which clearly underlines the CS character for such an excited state of all three investigated dyads.

The T_1 state geometry of the dyads in CHX was also optimized (Figure 10). For **PTZ-Ph-AQ** and **PTZ-PhMe-AQ**, all of the α, β, and γ dihedral angles are very similar to those calculated for the S_1 state, suggesting the CS nature of the T_1 states of these dyads. The analysis of the NTOs for the T_1 states of both **PTZ-Ph-AQ** and **PTZ-PhMe-AQ** dyads also underline the same CS character as for S_1. On the other hand, significant differences are obtained for **PTZ-Ph$_2$Me-AQ**. The α dihedral angle increases to 100°, which is 8.9 and 2.3° larger than that calculated for the S_1 and S_0 states, respectively, while β is calculated to be −114.1°, which is 5.4° and 22.5° smaller than that computed for S_1 and S_0 states, respectively. Interestingly, the optimized structure of the T_1 state shows that the puckered geometry of the PTZ is restored, with a calculated value of γ of 35.8°, which is very similar to that of the compound in its gas-phase ground state. Due to the different dihedral angles calculated for the S_1 and T_1 for **PTZ-Ph$_2$Me-AQ**, a different nature of the transition might be expected. This hypothesis is confirmed by the NTO analysis, which shows indeed that the T_1 state involves a LE transition involving the AQ part of the dyad (Figure 11).

The ISC is supposed to occur from the lowest lying singlet state ^{1}CS and to the triplet state with the closest energy. Both the **PTZ-Ph-AQ** and **PTZ-PhMe-AQ** dyads show similar energy with the T_1 and T_2 states lying below and above the S_1 state, respectively. On the other hand, for **PTZ-Ph$_2$Me-AQ**, both T_1 and T_2 states are found to be lower energy than the S_1 state energy. The calculated energies of the S_1, T_1, and T_2 states for both **PTZ-Ph-AQ** and **PTZ-PhMe-AQ** are very similar, indicating that the inclusion of the two methyl groups on the phenylene linker, though affects the geometry (especially the β dihedral angle), does not influence the energies and ordering of the relevant excited states. The addition of the second phenylene group in **PTZ-Ph$_2$Me-AQ** increases the energy of the S_1 and T_1 states by >0.4 and >0.1 eV, respectively (Table 3). To characterize the nature of these states, we performed natural transition orbital (NTO) analysis (Figure 11),[97] which shows that the S_1 and T_1 excitations in both **PTZ-Ph-AQ** and **PTZ-PhMe-AQ** appear to be dominated by HOTO (highest occupied transition orbital) to LUTO (lowest unoccupied transition orbital) excitations, showing CS from the donor PTZ to the acceptor AQ, while the S_0−T_2 transition is LE-like and involves the AQ part of the dyad. Moreover, the increase of the torsion angle between the linker and the AQ part due to the presence of the methyl substituents further decreases the extent of the orbitals' overlap between the two moieties, enhancing the CS character of the S_1 and T_1 states and therefore slightly reducing the ΔE_{ST} (Table 3). The ΔE_{ST} values of **PTZ-Ph-AQ** and **PTZ-PhMe-AQ** are dramatically small and T_1 and S_1 states can be considered degenerate. On the other hand, for the **PTZ-Ph$_2$Me-AQ** compound, the T_1 excitation involves a LE transition on the AQ moiety, while the nature of the S_1, T_2, and T_3 transitions is CS from the PTZ donor to the AQ acceptor. The largest ΔE_{ST} obtained for **PTZ-Ph$_2$Me-AQ** (0.30 eV) is in line with the LE character of the T_1 state found for this compound.

The molecules exhibiting TADF are characterized by small singlet−triplet energy gaps that help rISC. On the basis of these results, we propose that the TADF process observed in **PTZ-Ph-AQ** and, to a lesser extent, in **PTZ-PhMe-AQ** occurs by an ISC between S_1 and T_2 states, with a $\Delta E(^1\text{CS}-^3\text{LE})$ of −0.11 and −0.16 eV, respectively. These transitions are favored by the spin−orbit coupling as supported by the calculated SOC of 0.12 cm^{-1}. An internal conversion (IC) process, with a $\Delta E(^3\text{LE}/^3\text{CS})$ of 0.11 and 0.16 eV, for **PTZ-Ph-AQ** and **PTZ-PhMe-AQ**, respectively, converts the T_2 (^{3}LE) into the T_1 (^{3}CS), which is eventually involved in the rISC with the $T_1 \rightarrow {}^1$CS. However, the $\Delta E(^1\text{CS}/^3\text{LE})$ is larger in **PTZ-Ph$_2$Me-AQ** (0.30 eV) than those of **PTZ-Ph-AQ** (0.11 eV) and **PTZ-PhMe-AQ** (0.16 eV), and the SOC value between ^{1}CS and ^{3}LE is very small in **PTZ-Ph$_2$Me-AQ** (0.04 cm^{-1}); thus, the ISC process of $^1\text{CS}\rightarrow T_1$ is inefficient in **PTZ-**

https://doi.org/10.1021/acs.jpcb.3c02723
J. Phys. Chem. B XXXX, XXX, XXX−XXX

Ph_2Me-AQ. Moreover, T_2 and T_3 states are CS nature in **PTZ-Ph_2Me-AQ**, and the rISC process of ^{3}CS → ^{1}CS is also inefficient, because of no change in angular mometum between ^{1}CS and ^{3}CS states with similar electronic configuration. These results were supported by the experiments, and no TADF was observed in **PTZ-Ph_2Me-AQ**. On the other hand, the lower $\Delta E(^1\text{CS}/^3\text{LE})$ and $\Delta E(^3\text{LE}/^3\text{CS})$, along with the higher SOC values calculated for **PTZ-Ph-AQ** and **PTZ-PhMe-AQ**, agree with the TADF observed experimentally for both those dyads. Moreover, the small energy gap $\Delta E(^3\text{LE}/^3\text{CS})$ in those compounds and not in the case of PTZ-Ph2Me-AQ supports the possibility that vibronic coupling plays a role in promoting the rISC only in those cases.[98]

Based on the above results, we constructed the simplified Jablonski diagram to explain the photophysical processes of the dyads (Figure 12). The energy levels for singlet/triplet excited states of the compounds are obtained by DFT computations. Upon photoexcitation of **PTZ-Ph-AQ**, the singlet excited state of the dyad is populated. Then, electron transfer occurs to produce the ^{1}CS state, and the CS takes 1 ps for **PTZ-Ph-AQ** in CHX. The ^{3}CS state presents a long lifetime as observed in ns-TA spectra (7.0 μs). Due to the closely lying ^{1}CS (2.11 eV) and ^{3}CS states (2.11 eV), the rISC is also taking place in this compound and TADF is observed, with a long-lived fluorescence lifetime in N_2 purged CHX (62.0 ns (99.2%)/ 7.6 μs (0.8%)). **PTZ-PhMe-AQ** has similar photophysical processes. For **PTZ-Ph_2Me-AQ**, upon photoexcitation, electron transfer takes place from PTZ to AQ (3 ps), followed by the population of the ^{3}AQ* state. Experiments and DFT calculations show that the two-state model may be non-sufficient to explain TADF; rather, a close-lying ^{3}LE state should be involved in TADF.

4. CONCLUSIONS

In summary, in order to study the electron transfer and intersystem crossing in compact electron donor−acceptor dyads and the relationship between the molecular structure and the thermally activated delayed fluorescence (TADF) property of the dyads, we prepared a series of phenothiazine (PTZ)−anthraquinone (AQ) electron donor−acceptor dyads using *p*-phenylene and *p*-biphenylene linkers. The single-crystal molecular structure showed that the PTZ unit adopts a puckered geometry in the ground state. The UV−vis absorption spectra showed that **PZT-Ph-AQ** has a charge transfer (CT) absorption band centered at 418 nm, indicating electronic coupling between the donor and acceptor in the ground state, whereas this CT absorption band vanished in the dyads having either conformation restriction or larger distance between the donor and acceptor. We found significant TADF for the dyad containing a *p*-phenylene linker; the prompt fluorescence lifetime is 62 ns (population ratio: 99.2%) and the delayed fluorescence lifetime is 7.6 μs (0.8%). In comparison, a previously reported dyad without the intervening phenylene linker does not show any TADF property. In the analogous dyad with conformation restriction exerted by the methyl groups attached on the phenylene linker, an unusually long prompt fluorescence lifetime of 245 ns (93.5%) was observed, and the delayed fluorescence lifetime was 2.4 μs (6.5%). In the dyad containing *p*-biphenylene linker, no TADF was observed although a long-lived CS state was detected with nanosecond transient absorption (CS state lifetimes are 1.8 and 1.3 μs in cyclohexane and acetonitrile, respectively), because of the elevated CS state energy (2.50 eV) as compared to the triplet state energy (ca. 2.25 eV). The CS state was observed with nanosecond transient absorption spectroscopy, and the CS state lifetimes of the two dyads containing a *p*-phenylene linker are in the range of 104 ns to 7.0 μs (the lifetime is shorter in polar solvents). These experimental results show that even if a long-lived CS state is populated, no TADF will occur if the ^{3}LE lies well above the CS state or below the CS state. Density functional theory (DFT)/time-dependent density functional theory (TD-DFT) calculations show that the optimized geometry of the PTZ in the dyads can aid the assignment of the transient species as either a ^{3}LE state or a ^{3}CS state. Femtosecond transient absorption spectra show that charge separation (CS) occurs readily (takes 1−5 ps) for most dyads also in nonpolar solvents, with the ^{1}AQ state as a precursor. Nanosecond pulsed laser-excited time-resolved electron paramagnetic resonance (TREPR) spectra show that the spin-correlated radical pair (SCRP) was formed, with the electron exchange energy $2J$ = +2.14 mT, or radical pairs with stronger interaction, $|2J|$ > 6.57 mT. These studies are useful for in-depth understanding of the charge separation and intersystem crossing in compact electron donor−acceptor dyads and for design of efficient TADF emitters.

■ ASSOCIATED CONTENT

Supporting Information

The Supporting Information is available free of charge at https://pubs.acs.org/doi/10.1021/acs.jpcb.3c02723.

General experimental methods, synthesis of compounds, molecular structure characterization, computational details, and additional spectra (PDF)

■ AUTHOR INFORMATION

Corresponding Authors

Jianzhang Zhao − *State Key Laboratory of Fine Chemicals, Frontiers Science Center for Smart Materials, School of Chemical Engineering, Dalian University of Technology, Dalian 116024, P. R. China; State Key Laboratory of Chemistry and Utilization of Carbon Based Energy Resources, College of Chemistry, Xinjiang University, Urumqi 830017, P. R. China;* orcid.org/0000-0002-5405-6398; Email: zhaojzh@dlut.edu.cn

Violeta K. Voronkova − *Zavoisky Physical-Technical Institute, FRC Kazan Scientific Center of Russian Academy of Sciences, Kazan 420029, Russia*; Email: vor18@yandex.ru

Mariangela Di Donato − *LENS (European Laboratory for Non-Linear Spectroscopy), 50019 Sesto Fiorentino, Florence, Italy; ICCOM-CNR, 50019 Sesto Fiorentino, Florence, Italy;* orcid.org/0000-0002-6596-7031; Email: didonato@lens.unifi.it

Gloria Mazzone − *Dipartimento di Chimica e Tecnologie Chimiche, Università della Calabria, I-87036 Arcavacata di Rende, Italy*; Email: gloria.mazzone@unical.it

Authors

Zhibin Yu − *State Key Laboratory of Fine Chemicals, Frontiers Science Center for Smart Materials, School of Chemical Engineering, Dalian University of Technology, Dalian 116024, P. R. China*

Andrey A. Sukhanov − *Zavoisky Physical-Technical Institute, FRC Kazan Scientific Center of Russian Academy of Sciences, Kazan 420029, Russia*

https://doi.org/10.1021/acs.jpcb.3c02723
J. Phys. Chem. B XXXX, XXX, XXX−XXX

Xiao Xiao − *State Key Laboratory of Fine Chemicals, Frontiers Science Center for Smart Materials, School of Chemical Engineering, Dalian University of Technology, Dalian 116024, P. R. China*

Alessandro Iagatti − *LENS (European Laboratory for Non-Linear Spectroscopy), 50019 Sesto Fiorentino, Florence, Italy; INO-CNR (Istituto Nazionale di Ottica-Consiglio Nazionale delle Ricerche), 50125 Firenze, Florence, Italy*

Sandra Doria − *LENS (European Laboratory for Non-Linear Spectroscopy), 50019 Sesto Fiorentino, Florence, Italy; ICCOM-CNR, 50019 Sesto Fiorentino, Florence, Italy;* orcid.org/0000-0002-9440-1643

Valeria Butera − *CEITEC-Central European Institute of Technology, Brno University of Technology, Brno 612 00, Czech Republic*

Complete contact information is available at: https://pubs.acs.org/10.1021/acs.jpcb.3c02723

Author Contributions

◆Z.Y. and A.A.S. and X.X. contributed equally to this work.

Notes

The authors declare no competing financial interest.

■ ACKNOWLEDGMENTS

J.Z. would like to thank the NSFC (U2001222), the Research and Innovation Team Project of Dalian University of Technology (DUT2022TB10), the Fundamental Research Funds for the Central Universities (DUT22LAB610), and the State Key Laboratory of Fine Chemicals for financial support. A.A.S. and V.K.V. acknowledge financial support from the government assignment for FRC Kazan Scientific Centre of RAS. M.D.D. would like to thank the European Union's Horizon 2020 research and innovation program under grant agreement no. 871124 Laserlab, Europe, for the support.

■ REFERENCES

(1) Guldi, D. M. Fullerenes: Three Dimensional Electron Acceptor Materials. *Chem. Commun.* **2000**, 321−327.

(2) Fukuzumi, S. New Perspective of Electron Transfer Chemistry. *Org. Biomol. Chem.* **2003**, *1*, 609−620.

(3) Verhoeven, J. W. On the Role of Spin Correlation in the Formation, Decay, and Detection of Long-Lived, Intramolecular Charge-Transfer States. *J. Photochem. Photobiol., C* **2006**, *7*, 40−60.

(4) Ohkubo, K.; Shunichi, F. Rational Design and Functions of Electron Donor−Acceptor Dyads with Much Longer Charge-Separated Lifetimes than Natural Photosynthetic Reaction Centers. *Bull. Chem. Soc. Jpn.* **2009**, *82*, 303−315.

(5) Suzuki, S.; Kozaki, M.; Nozaki, K.; Okada, K. Recent Progress in Controlling Photophysical Processes of Donor−Acceptor Arrays Involving Perylene Diimides and Boron-Dipyrromethenes. *J. Photochem. Photobiol., C* **2011**, *12*, 269−292.

(6) Blas-Ferrando, V. M.; Ortiz, J.; Ohkubo, K.; Fukuzumi, S.; Fernández-Lázaro, F.; Sastre-Santos, A. Submillisecond-Lived Photoinduced Charge Separation in a Fully Conjugated Phthalocyanine−Perylenebenzimidazole Dyad. *Chem. Sci.* **2014**, *5*, 4785−4793.

(7) Scattergood, P. A.; Delor, M.; Sazanovich, I. V.; Towrie, M.; Weinstein, J. A. Ultrafast Charge Transfer Dynamics in Supramolecular Pt(II) Donor−Bridge−Acceptor Assemblies: The Effect of Vibronic Coupling. *Faraday. Discuss.* **2015**, *185*, 69−86.

(8) Purc, A.; Espinoza, E. M.; Nazir, R.; Romero, J. J.; Skonieczny, K.; Jeżewski, A.; Larsen, J. M.; Gryko, D. T.; Vullev, V. I. Gating That Suppresses Charge Recombination−The Role of Mono-N-Arylated Diketopyrrolopyrrole. *J. Am. Chem. Soc.* **2016**, *138*, 12826−12832.

(9) Hu, W.; Liu, M.; Zhang, X.-F.; Wang, Y.; Wang, Y.; Lan, H.; Zhao, H. Can BODIPY-Electron Acceptor Conjugates Act as Heavy Atom-Free Excited Triplet State and Singlet Oxygen Photosensitizers via Photoinduced Charge Separation-Charge Recombination Mechanism? *J. Phys. Chem. C* **2019**, *123*, 15944−15955.

(10) Shao, S.; Gobeze, H. B.; Bandi, V.; Funk, C.; Heine, B.; Duffy, M. J.; Nesterov, V.; Karr, P. A.; D'Souza, F. Triplet BODIPY and AzaBODIPY Derived Donor-Acceptor Dyads: Competitive Electron Transfer Versus Intersystem Crossing upon Photoexcitation. *ChemPhotoChem* **2020**, *4*, 68−81.

(11) Kong, J.; Zhang, W.; Shao, J.-Y.; Huo, D.; Niu, X.; Wan, Y.; Song, D.; Zhong, Y.-W.; Xia, A. Bridge-Length- and Solvent-Dependent Charge Separation and Recombination Processes in Donor−Bridge−Acceptor Molecules. *J. Phys. Chem. B* **2021**, *125*, 13279−13290.

(12) Imahori, H.; Kobori, Y.; Kaji, H. Manipulation of Charge-Transfer States by Molecular Design: Perspective from "Dynamic Exciton". *Acc. Mater. Res.* **2021**, *2*, 501−514.

(13) Gust, D.; Moore, T. A.; Moore, A. L. Molecular Mimicry of Photosynthetic Energy and Electron Transfer. *Acc. Chem. Res.* **1993**, *26*, 198−205.

(14) Chakraborty, S.; Wadas, T. J.; Hester, H.; Schmehl, R.; Eisenberg, R. Platinum Chromophore-Based Systems for Photoinduced Charge Separation: A Molecular Design Approach for Artificial Photosynthesis. *Inorg. Chem.* **2005**, *44*, 6865−6878.

(15) Fukuzumi, S. New Development of Photoinduced Electron-Transfer Catalytic Systems. *Pure Appl. Chem.* **2007**, *79*, 981−991.

(16) Veldkamp, B. S.; Han, W.-S.; Dyar, S. M.; Eaton, S. W.; Ratner, M. A.; Wasielewski, M. R. Photoinitiated Multi-Step Charge Separation and Ultrafast Charge Transfer Induced Dissociation in a Pyridyl-Linked Photosensitizer−Cobaloxime Assembly. *Energy Environ. Sci.* **2013**, *6*, 1917−1928.

(17) Luo, G.-G.; Fang, K.; Wu, J.-H.; Mo, J. Photocatalytic Water Reduction from a Noble-Metal-Free Molecular Dyad Based on a Thienyl-Expanded BODIPY Photosensitizer. *Chem. Commun.* **2015**, *51*, 12361−12364.

(18) Chergui, M. Ultrafast Photoinduced Energy and Charge Transfer. *Faraday. Discuss.* **2019**, *216*, 9−37.

(19) Chen, K.-Y.; Hsieh, C.-C.; Cheng, Y.-M.; Lai, C.-H.; Chou, P.-T.; Chow, T. J. Tuning Excited-State Electron Transfer from an Adiabatic to Nonadiabatic Type in Donor−Bridge−Acceptor Systems and the Associated Energy-Transfer Process. *J. Phys. Chem. A* **2006**, *110*, 12136−12144.

(20) Higashino, T.; Yamada, T.; Yamamoto, M.; Furube, A.; Tkachenko, N. V.; Miura, T.; Kobori, Y.; Jono, R.; Yamashita, K.; Imahori, H. Remarkable Dependence of the Final Charge Separation Efficiency on the Donor−Acceptor Interaction in Photoinduced Electron Transfer. *Angew. Chem., Int. Ed.* **2016**, *55*, 629−633.

(21) Ziessel, R.; Allen, B. D.; Rewinska, D. B.; Harriman, A. Selective Triplet-State Formation during Charge Recombination in a Fullerene/Bodipy Molecular Dyad (Bodipy = Borondipyrromethene). *Chem. - Eur. J.* **2009**, *15*, 7382−7393.

(22) Suneesh, C. V.; Gopidas, K. R. Long-Lived Photoinduced Charge Separation Due to the Inverted Region Effect in 1,6-Bis(phenylethynyl)pyrene−Phenothiazine Dyad. *J. Phys. Chem. C* **2010**, *114*, 18725−18734.

(23) Bandi, V.; Gobeze, H. B.; Lakshmi, V.; Ravikanth, M.; D'Souza, F. Vectorial Charge Separation and Selective Triplet-State Formation during Charge Recombination in a Pyrrolyl-Bridged BODIPY−Fullerene Dyad. *J. Phys. Chem. C* **2015**, *119*, 8095−8102.

(24) Anglos, D.; Bindra, V.; Kuki, A. Photoinduced Electron Transfer and Long-Lived Charge Separation in Rigid Peptide Architectures. *J. Chem. Soc., Chem. Commun.* **1994**, 213−215.

(25) van Dijk, S. I.; Groen, C. P.; Hartl, F.; Brouwer, A. M.; Verhoeven, J. W. Long-Lived Triplet State Charge Separation in Novel Piperidine-Bridged Donor−Acceptor Systems. *J. Am. Chem. Soc.* **1996**, *118*, 8425−8432.

(26) Hviid, L.; Brouwer, A. M.; Paddon-Row, M. N.; Verhoeven, J. W. Long-Lived Short-Distance Intramolecular Charge Separation via Intermolecular Triplet Sensitisation. *ChemPhysChem* **2001**, *2*, 232−235.

(27) Geiß, B.; Lambert, C. A Small Cationic Donor−Acceptor Iridium Complex with a Long-Lived Charge-Separated State. *Chem. Commun.* **2009**, 1670−1672.
(28) Murakami, M.; Ohkubo, K.; Nanjo, T.; Souma, K.; Suzuki, N.; Fukuzumi, S. Photoinduced Electron Transfer in Photorobust Coumarins Linked with Electron Donors Affording Long Lifetimes of Triplet Charge-Separated States. *ChemPhysChem* **2010**, *11*, 2594−2605.
(29) Hankache, J.; Wenger, O. S. Microsecond Charge Recombination in a Linear Triarylamine−Ru(bpy)$_3^{2+}$−Anthraquinone Triad. *Chem. Commun.* **2011**, *47*, 10145−10147.
(30) Subedi, D. R.; Gobeze, H. B.; Kandrashkin, Y. E.; Poddutoori, P. K.; van der Est, A.; D'Souza, F. Exclusive Triplet Electron Transfer Leading to Long-Lived Radical Ion-Pair Formation in an Electron Rich Platinum Porphyrin Covalently Linked to Fullerene Dyad. *Chem. Commun.* **2020**, *56*, 6058−6061.
(31) Zarrabi, N.; Bayard, B. J.; Seetharaman, S.; Holzer, N.; Karr, P.; Ciuti, S.; Barbon, A.; Di Valentin, M.; van der Est, A.; D'Souza, F.; Poddutoori, P. K. A Charge Transfer State Induced by Strong Exciton Coupling in a Cofacial μ-Oxo-Bridged Porphyrin Heterodimer. *Phys. Chem. Chem. Phys.* **2021**, *23*, 960−970.
(32) Verhoeven, J. W.; van Ramesdonk, H. J.; Groeneveld, M. M.; Benniston, A. C.; Harriman, A. Long-Lived Charge-Transfer States in Compact Donor−Acceptor Dyads. *ChemPhysChem* **2005**, *6*, 2251−2260.
(33) Liu, D.; El-Zohry, A. M.; Taddei, M.; Matt, C.; Bussotti, L.; Wang, Z.; Zhao, J.; Mohammed, O. F.; Di Donato, M.; Weber, S. Long-Lived Charge-Transfer State Induced by Spin-Orbit Charge Transfer Intersystem Crossing (SOCT-ISC) in a Compact Spiro Electron Donor/Acceptor Dyad. *Angew. Chem., Int. Ed.* **2020**, *59*, 11591−11599.
(34) Chen, X.; Sukhanov, A. A.; Yan, Y.; Bese, D.; Bese, C.; Zhao, J.; Voronkova, V. K.; Barbon, A.; Yaglioglu, H. G. Long-Lived Charge-Transfer State in Spiro Compact Electron Donor−Acceptor Dyads Based on Pyromellitimide-Derived Rhodamine: Charge Transfer Dynamics and Electron Spin Polarization. *Angew. Chem., Int. Ed.* **2022**, *61*, No. e202203758.
(35) Harriman, A.; Mallon, L. J.; Ulrich, G.; Ziessel, R. Rapid Intersystem Crossing in Closely-Spaced but Orthogonal Molecular Dyads. *ChemPhysChem* **2007**, *8*, 1207−1214.
(36) Epelde-Elezcano, N.; Palao, E.; Manzano, H.; Prieto-Castañeda, A.; Agarrabeitia, A. R.; Tabero, A.; Villanueva, A.; de la Moya, S.; de la Moya, S.; López-Arbeloa, Í.; Martínez-Martínez, V. Rational Design of Advanced Photosensitizers Based on Orthogonal BODIPY Dimers to Finely Modulate Singlet Oxygen Generation. *Chem. - Eur. J.* **2017**, *23*, 4837−4848.
(37) Hou, Y.; Zhang, X.; Chen, K.; Liu, D.; Wang, Z.; Liu, Q.; Zhao, J.; Barbon, A. Charge Separation, Charge Recombination, Long-Lived Charge Transfer State Formation and Intersystem Crossing in Organic Electron Donor/Acceptor Dyads. *J. Mater. Chem. C* **2019**, *7*, 12048−12074.
(38) Gibbons, D. J.; Farawar, A.; Mazzella, P.; Leroy-Lhez, S.; Williams, R. M. Making Triplets from Photo-Generated Charges: Observations, Mechanisms and Theory. *Photochem. Photobiol. Sci.* **2020**, *19*, 136−158.
(39) Filatov, M. A. Heavy-Atom-Free BODIPY Photosensitizers with Intersystem Crossing Mediated by Intramolecular Photoinduced Electron Transfer. *Org. Biomol. Chem.* **2020**, *18*, 10−27.
(40) Bassan, E.; Gualandi, A.; Cozzi, P. G.; Ceroni, P. Design of BODIPY Dyes as Triplet Photosensitizers: Electronic Properties Tailored for Solar Energy Conversion, Photoredox Catalysis and Photodynamic Therapy. *Chem. Sci.* **2021**, *12*, 6607−6628.
(41) Zhang, X.; Zhao, X.; Ye, K.; Zhao, J. Detection of the Dark States in Thermally Activated Delayed Fluorescence (TADF) Process of Electron Donor-Acceptor Dyads: Insights from Optical Transient Absorption Spectroscopy. *Chem. - Eur. J.* **2023**, *29*, No. e202203737.
(42) Tao, Y.; Yuan, K.; Chen, T.; Xu, P.; Li, H.; Chen, R.; Zheng, C.; Zhang, L.; Huang, W. Thermally Activated Delayed Fluorescence Materials Towards the Breakthrough of Organoelectronics. *Adv. Mater.* **2014**, *26*, 7931−7958.
(43) Im, Y.; Byun, S. Y.; Kim, J. H.; Lee, D. R.; Oh, C. S.; Yook, K. S.; Lee, J. Y. Recent Progress in High-Efficiency Blue-Light-Emitting Materials for Organic Light-Emitting Diodes. *Adv. Funct. Mater.* **2017**, *27*, No. 1603007.
(44) Yang, Z.; Mao, Z.; Xie, Z.; Zhang, Y.; Liu, S.; Zhao, J.; Xu, J.; Chi, Z.; Aldred, M. P. Recent Advances in Organic Thermally Activated Delayed Fluorescence Materials. *Chem. Soc. Rev.* **2017**, *46*, 915−1016.
(45) Ni, F.; Li, N.; Zhan, L.; Yang, C. Organic Thermally Activated Delayed Fluorescence Materials for Time-Resolved Luminescence Imaging and Sensing. *Adv. Opt. Mater.* **2020**, *8*, No. 1902187.
(46) Xu, Y.; Xu, P.; Hu, D.; Ma, Y. Recent Progress in Hot Exciton Materials for Organic Light-Emitting Diodes. *Chem. Soc. Rev.* **2021**, *50*, 1030−1069.
(47) Chen, L.; Chen, W.-C.; Yang, Z.; Tan, J.-H.; Ji, S.; Zhang, H.-L.; Huo, Y.; Lee, C.-S. Triplet Harvesting Aryl Carbonyl-Based Luminescent Materials: Progress and Prospective. *J. Mater. Chem. C* **2021**, *9*, 17233−17264.
(48) Hosokai, T.; Matsuzaki, H.; Nakanotani, H.; Tokumaru, K.; Tsutsui, T.; Furube, A.; Nasu, K.; Nomura, H.; Yahiro, M.; Adachi, C. Evidence and Mechanism of Efficient Thermally Activated Delayed Fluorescence Promoted by Delocalized Excited States. *Sci. Adv.* **2017**, *3*, No. e1603282.
(49) Zhang, W.; Song, H.; Kong, J.; Kuang, Z.; Li, M.; Guo, Q.; Chen, C.-f.; Xia, A. Importance of Conformational Change in Excited States for Efficient Thermally Activated Delayed Fluorescence. *J. Phys. Chem. C* **2019**, *123*, 19322−19332.
(50) Drummond, B. H.; Aizawa, N.; Zhang, Y.; Myers, W. K.; Xiong, Y.; Cooper, M. W.; Barlow, S.; Gu, Q.; Weiss, L. R.; Gillett, A. J.; et al. W. Electron Spin Resonance Resolves Intermediate Triplet States in Delayed Fluorescence. *Nat. Commun.* **2021**, *12*, No. 4532.
(51) Tanaka, H.; Shizu, K.; Miyazaki, H.; Adachi, C. Efficient Green Thermally Activated Delayed Fluorescence (TADF) from a Phenoxazine−Triphenyltriazine (PXZ−TRZ) Derivative. *Chem. Commun.* **2012**, *48*, 11392−11394.
(52) Peng, Q.; Fan, D.; Duan, R.; Yi, Y.; Niu, Y.; Wang, D.; Shuai, Z. Theoretical Study of Conversion and Decay Processes of Excited Triplet and Singlet States in a Thermally Activated Delayed Fluorescence Molecule. *J. Phys. Chem. C* **2017**, *121*, 13448−13456.
(53) Etherington, M. K.; Gibson, J.; Higginbotham, H. F.; Penfold, T. J.; Monkman, A. P. Revealing the Spin−Vibronic Coupling Mechanism of Thermally Activated Delayed Fluorescence. *Nat. Commun.* **2016**, *7*, No. 13680.
(54) Dias, F. B.; Penfold, T. J.; Monkman, A. P. Photophysics of Thermally Activated Delayed Fluorescence Molecules. *Methods Appl. Fluoresc.* **2017**, *5*, No. 012001.
(55) Kim, I.; Jeon, S. O.; Jeong, D.; Choi, H.; Son, W.-J.; Kim, D.; Rhee, Y. M.; Lee, H. S. Spin−Vibronic Model for Quantitative Prediction of Reverse Intersystem Crossing Rate in Thermally Activated Delayed Fluorescence Systems. *J. Chem. Theory Comput.* **2020**, *16*, 621−632.
(56) Kim, I.; Cho, K. H.; Jeon, S. O.; Son, W.-J.; Kim, D.; Rhee, Y. M.; Jang, I.; Choi, H.; Kim, D. S. Three States Involving Vibronic Resonance is a Key to Enhancing Reverse Intersystem Crossing Dynamics of an Organoboron-Based Ultrapure Blue Emitter. *JACS Au* **2021**, *1*, 987−997.
(57) Lin, S.; Pei, Z.; Zhang, B.; Ma, H.; Liang, W. Vibronic Coupling Effect on the Vibrationally Resolved Electronic Spectra and Intersystem Crossing Rates of a TADF Emitter: 7-PhQAD. *J. Phys. Chem. A* **2022**, *126*, 239−248.
(58) Zhong, F.; Zhao, J.; Hayvali, M.; Elmali, A.; Karatay, A. Effect of Molecular Conformation Restriction on the Photophysical Properties of N∧N Platinum(II) Bis(ethynylnaphthalimide) Complexes Showing Close-Lying ^{3}MLCT and ^{3}LE Excited States. *Inorg. Chem.* **2019**, *58*, 1850−1861.
(59) Tang, G.; Sukhanov, A. A.; Zhao, J.; Yang, W.; Wang, Z.; Liu, Q.; Voronkova, V. K.; Di Donato, M.; Escudero, D.; Jacquemin, D.

https://doi.org/10.1021/acs.jpcb.3c02723
J. Phys. Chem. B XXXX, XXX, XXX−XXX

Red Thermally Activated Delayed Fluorescence and the Intersystem Crossing Mechanisms in Compact Naphthalimide−Phenothiazine Electron Donor/Acceptor Dyads. *J. Phys. Chem. C* **2019**, *123*, 30171−30186.
(60) Zhou, F.; Shao, J.; Yang, Y.; Zhao, J.; Guo, H.; Li, X.; Ji, S.; Zhang, Z. Molecular Rotors as Fluorescent Viscosity Sensors: Molecular Design, Polarity Sensitivity, Dipole Moments Changes, Screening Solvents, and Deactivation Channel of the Excited States. *Eur. J. Org. Chem.* **2011**, *2011*, 4773−4787.
(61) Snellenburg, J. J.; Laptenok, S.; Seger, R.; Mullen, K. M.; van Stokkum, I. H. M. Glotaran: A Java-Based Graphical User Interface for the R Package TIMP. *J. Stat. Software* **2012**, *49*, 1−22.
(62) Stoll, S.; Schweiger, A. EasySpin, a Comprehensive Software Package for Spectral Simulation and Analysis in EPR. *J. Magn. Reson.* **2006**, *178*, 42−55.
(63) Dolomanov, O. V.; Bourhis, L. J.; Gildea, R. J.; Howard, J. A. K.; Puschmann, H. OLEX2: A Complete Structure Solution, Refinement and Analysis Program. *J. Appl. Crystallogr.* **2009**, *42*, 339−341.
(64) Adamo, C.; Jacquemin, D. The Calculations of Excited-State Properties with Time-Dependent Density Functional Theory. *Chem. Soc. Rev.* **2013**, *42*, 845−856.
(65) Laurent, A. D.; Jacquemin, D. TD-DFT Benchmarks: A Review. *Int. J. Quantum. Chem.* **2013**, *113*, 2019−2039.
(66) Butera, V.; Detz, H. Photochemical CO_2 Conversion on Pristine and Mg-Doped Gallium Nitride (GaN): a Comprehensive DFT Study Based on a Cluster Model Approach. *Mater. Chem. Front.* **2021**, *5*, 8206−8217.
(67) Rohman, S.; Kar, R. Excited-State Properties of Some Thermally Activated Delayed Fluorescence Emitters: Quest for an Accurate and Reliable Computational Method. *J. Phys. Chem. A* **2022**, *126*, 3452−3462.
(68) Bransden, B. H. Many Particle Systems. *Nature* **1971**, *232*, 139−140.
(69) Peach, M. J. G.; Williamson, M. J.; Tozer, D. J. Influence of Triplet Instabilities in TDDFT. *J. Chem. Theory Comput.* **2011**, *7*, 3578−3585.
(70) Peach, M. J. G.; Tozer, D. J. Overcoming Low Orbital Overlap and Triplet Instability Problems in TDDFT. *J. Phys. Chem. A* **2012**, *116*, 9783−9789.
(71) Peach, M. J. G.; Warner, N.; Tozer, D. J. On the Triplet Instability in TDDFT. *Mol. Phys.* **2013**, *111*, 1271−1274.
(72) Butera, V.; Mazzone, G.; Detz, H. Dinuclear Ruthenium(II)-Pyrrolide Complexes Linked by Different Organic Units as PDT Photosensitizers: Computational Study of the Linker Influence on the Photophysical Properties. *ChemPhotoChem* **2022**, *6*, No. e202200094.
(73) van Ramesdonk, H. J.; Bakker, B. H.; Groeneveld, M. M.; Verhoeven, J. W.; Allen, B. D.; Rostron, J. P.; Harriman, A. Ultrafast Intersystem Crossing in 9,10-Anthraquinones and Intramolecular Charge Separation in an Anthraquinone-Based Dyad. *J. Phys. Chem. A* **2006**, *110*, 13145−13150.
(74) Huang, B.; Chen, W.-C.; Li, Z.; Zhang, J.; Zhao, W.; Feng, Y.; Tang, B. Z.; Lee, C.-S. Manipulation of Molecular Aggregation States to Realize Polymorphism, AIE, MCL, and TADF in a Single Molecule. *Angew. Chem., Int. Ed.* **2018**, *57*, 12473−12477.
(75) Zhao, X.; Sukhanov, A. A.; Jiang, X.; Zhao, J.; Voronkova, V. K. Long-Lived Triplet Charge Separated State and Thermally Activated Delayed Fluorescence in a Compact Orthogonal Anthraquinone−Phenothiazine Electron Donor−Acceptor Dyad. *J. Phys. Chem. Lett.* **2022**, *13*, 2533−2539.
(76) Kuss-Petermann, M.; Wenger, O. S. Increasing Electron-Transfer Rates with Increasing Donor−Acceptor Distance. *Angew. Chem., Int. Ed.* **2016**, *55*, 815−819.
(77) Karimata, A.; Kawauchi, H.; Suzuki, S.; Kozaki, M.; Ikeda, N.; Keyaki, K.; Nozaki, K.; Akiyama, K.; Okada, K. Photoinduced Charge Separation of 10-Phenyl-10H-phenothiazine−2-Phenylanthraquinone Dyad Bridged by Bicyclo[2.2.2]octane. *Chem. Lett.* **2013**, *42*, 794−796.
(78) Sasaki, S.; Hattori, K.; Igawa, K.; Konishi, G.-i. Directional Control of π-Conjugation Enabled by Distortion of the Donor Plane in Diarylaminoanthracenes: A Photophysical Study. *J. Phys. Chem. A* **2015**, *119*, 4898−4906.
(79) Dong, Y.; Sukhanov, A. A.; Zhao, J.; Elmali, A.; Li, X.; Dick, B.; Karatay, A.; Voronkova, V. K. Spin−Orbit Charge-Transfer Intersystem Crossing (SOCT-ISC) in Bodipy-Phenoxazine Dyads: Effect of Chromophore Orientation and Conformation Restriction on the Photophysical Properties. *J. Phys. Chem. C* **2019**, *123*, 22793−22811.
(80) Hou, Y.; Liu, J.; Zhang, N.; Zhao, J. Long-Lived Local Triplet Excited State and Charge Transfer State of 4,4′-Dimethoxy Triphenylamine-BODIPY Compact Electron Donor/Acceptor Dyads. *J. Phys. Chem. A* **2020**, *124*, 9360−9374.
(81) Zhao, X.; Zhao, J. Long-Lived Charge Separated State and Thermally Activated Delayed Fluorescence in Anthraquinone-Phenoxazine Electron Donor−Acceptor Dyads. *Chem. Commun.* **2022**, *58*, 7666−7669.
(82) Dance, Z. E. X.; Mi, Q.; McCamant, D. W.; Ahrens, M. J.; Ratner, M. A.; Wasielewski, M. R. Time-Resolved EPR Studies of Photogenerated Radical Ion Pairs Separated by *p*-Phenylene Oligomers and of Triplet States Resulting from Charge Recombination. *J. Phys. Chem. B* **2006**, *110*, 25163−25173.
(83) Shi, Y.-Z.; Wu, H.; Wang, K.; Yu, J.; Ou, X.-M.; Zhang, X.-H. Recent Progress in Thermally Activated Delayed Fluorescence Emitters for Nondoped Organic Light-Emitting Diodes. *Chem. Sci.* **2022**, *13*, 3625−3651.
(84) Montalti, M.; Credi, A.; Prodi, L.; Gandolfi, M. T. *Handbook of Photochemistry*; CRC Press: Boca Raton, 2006.
(85) Chen, X.; Xiao, X.; Zhao, J. Application of Time-Resolved Electron Paramagnetic Resonance Spectroscopy in the Mechanistic Study of Thermally Activated Delayed Fluorescence (TADF) Materials. *J. Mater. Chem. C* **2022**, *10*, 4546−4557.
(86) Goodson, F. S.; Panda, D. K.; Ray, S.; Mitra, A.; Guha, S.; Saha, S. Tunable Electronic Interactions between Anions and Perylenediimide. *Org. Biomol. Chem.* **2013**, *11*, 4797−4803.
(87) Guha, S.; Goodson, F. S.; Roy, S.; Corson, L. J.; Gravenmier, C. A.; Saha, S. Electronically Regulated Thermally and Light-Gated Electron Transfer from Anions to Naphthalenediimides. *J. Am. Chem. Soc.* **2011**, *133*, 15256−15259.
(88) Berera, R.; van Grondelle, R.; Kennis, J. T. M. Ultrafast Transient Absorption Spectroscopy: Principles and Application to Photosynthetic Systems. *Photosynth. Res.* **2009**, *101*, 105−118.
(89) Song, Q.; Zhang, X.; Ma, J.; Guo, Y.; Phillips, D. L. Time-Resolved Spectroscopic Study on the Photoredox Reaction of 2-(*p*-Hydroxymethyl)phenylAnthraquinone. *Sci. Rep.* **2017**, *7*, No. 9154.
(90) Imahori, H.; El-Khouly, M. E.; Fujitsuka, M.; Ito, O.; Sakata, Y.; Fukuzumi, S. Solvent Dependence of Charge Separation and Charge Recombination Rates in Porphyrin−Fullerene Dyad. *J. Phys. Chem. A* **2001**, *105*, 325−332.
(91) Yonemura, H.; Forbes, M. D. E. Electron Spin Exchange in Linked Phenothiazine−Viologen Charge Transfer Complexes Incorporated in "Through-Ring" (Rotaxane) α-Cyclodextrins. *Photochem. Photobiol.* **2015**, *91*, 672−677.
(92) Hintze, C.; Steiner, U. E.; Drescher, M. Photoexcited Triplet State Kinetics Studied by Electron Paramagnetic Resonance Spectroscopy. *ChemPhysChem* **2017**, *18*, 6−16.
(93) Biskup, T. Structure−Function Relationship of Organic Semiconductors: Detailed Insights from Time-Resolved EPR Spectroscopy. *Front. Chem.* **2019**, *7*, No. 10.
(94) Suzuki, S.; Sugimura, R.; Kozaki, M.; Keyaki, K.; Nozaki, K.; Ikeda, N.; Akiyama, K.; Okada, K. Highly Efficient Photoproduction of Charge-Separated States in Donor−Acceptor-Linked Bis(acetylide) Platinum Complexes. *J. Am. Chem. Soc.* **2009**, *131*, 10374−10375.
(95) Karimata, A.; Suzuki, S.; Kozaki, M.; Kimoto, K.; Nozaki, K.; Matsushita, H.; Ikeda, N.; Akiyama, K.; Kosumi, D.; Hashimoto, H.; Okada, K. Direct Observation of Hole Shift and Characterization of Spin States in Radical Ion Pairs Generated from Photoinduced

https://doi.org/10.1021/acs.jpcb.3c02723
J. Phys. Chem. B XXXX, XXX, XXX−XXX

Electron Transfer of (Phenothiazine)$_n$−Anthraquinone (n = 1, 3) Dyads. *J. Phys. Chem. A* **2014**, *118*, 11262−11271.
(96) Xiao, X.; Kurganskii, I.; Maity, P.; Zhao, J.; Jiang, X.; Mohammed, O. F.; Fedin, M. A. Long-Lived Charge-Separated State of Spiro Compact Electron Donor−Acceptor Dyads Based on Rhodamine and Naphthalenediimide Chromophores. *Chem. Sci.* **2022**, *13*, 13426−13441.
(97) Jayabharathi, J.; Thanikachalam, V.; Sundari, G. A. Efficient Electroluminescent Hybridized Local and Charge-Transfer Host Materials with Small Singlet−Triplet Splitting to Enhance Exciton Utilization Efficiency: Excited State Transition Configuration. *RSC Adv.* **2019**, *9*, 6658−6680.
(98) Gibson, J.; Monkman, A. P.; Penfold, T. J. The Importance of Vibronic Coupling for Efficient Reverse Intersystem Crossing in Thermally Activated Delayed Fluorescence Molecules. *ChemPhysChem* **2016**, *17*, 2956−2961.

https://doi.org/10.1021/acs.jpcb.3c02723
J. Phys. Chem. B XXXX, XXX, XXX−XXX